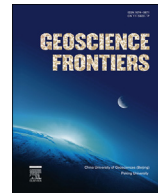




Contents lists available at ScienceDirect
China University of Geosciences (Beijing)

Geoscience Frontiers

journal homepage: www.elsevier.com/locate/gsf



Research Paper

An apatite U–Pb thermal history map for the northern Gawler Craton, South Australia

James W. Hall ^{a,*}, Stijn Glorie ^a, Anthony J. Reid ^{a,b}, Samuel C. Boone ^c, Alan S. Collins ^a, Andrew Gleadow ^c

^a Tectonics, Resources and Exploration (TRaX), Department of Earth Sciences, University of Adelaide, SA 5005, Australia

^b Geological Survey of South Australia, Department of State Development, GPO Box 1264, Adelaide, SA 5001, Australia

^c School of Earth Sciences, The University of Melbourne, Victoria, 3010, Australia

ARTICLE INFO

Article history:

Received 28 July 2017

Received in revised form

13 December 2017

Accepted 15 December 2017

Available online xxx

Keywords:

Apatite U–Pb

Gawler Craton

Karari Shear Zone

Thermochronology

Hiltaba event

ABSTRACT

Apatite U–Pb thermochronology was applied to granitoid basement samples across the northern Gawler Craton to unravel the Proterozoic, post-orogenic, cooling history and to examine the role of major fault zones during cooling. Our observations indicate that cooling following the ~2500 Ma Sleaford Orogeny and ~1700 Ma Kimban Orogeny is restricted to the Christie and Wilgena Domains of the central northern Gawler Craton. The northern Gawler Craton mainly records post-Hiltaba Event (~1590 Ma) U–Pb cooling ages. Cooling following the ~1560 Ma Kararan Orogeny is preserved within the Coober Pedy Ridge, Nawa Domain and along major shear zones within the south-western Fowler Domain. The Nawa Domain samples preserve U–Pb cooling ages that are >150 Ma younger than the samples within the Coober Pedy Ridge and Fowler Domain, indicating that later (~1300 Ma) fault movement within the Nawa Domain facilitated cooling of these samples, caused by arc collision in the Madura Province of eastern Western Australia. When compared to $^{40}\text{Ar}/^{39}\text{Ar}$ from muscovite, biotite and hornblende, our new apatite U–Pb ages correlate well, particularly in regions of higher data density. Our data also preserve a progressive younging of U–Pb ages from the nucleus of the craton to the periphery with a stark contrast in U–Pb ages across major structures such as the Karari Shear Zone and the Southern Overthrust, which indicates the timing of reactivation of these major crustal structures. Although this interpolation was based solely on thermochronological data and did not take into account structural or other geological data, these maps are consistent with the structural architecture of the Gawler Craton and reveal the thermal footprint of known tectonic and magmatic events in the Gawler Craton.

© 2018, China University of Geosciences (Beijing) and Peking University. Production and hosting by Elsevier B.V. This is an open access article under the CC BY-NC-ND license (<http://creativecommons.org/licenses/by-nc-nd/4.0/>).

1. Introduction

The duration and extent of tectonic events within a long-lived craton can be difficult to be determined (Daly et al., 1998; Hand et al., 2007). The difficulty is increased when major crustal structures are reactivated in different stress regimes by different tectonic events (e.g. Butler et al., 1997; Shaw et al., 2001; Williams and Betts, 2009), subsequently erasing evidence of older tectonic events. However, these structures play a key role in the longevity and stability of cratonic crust and influence their thermal histories. The chronology of these structures are often difficult to determine due

to factors such as outcrop availability, or difficulty in dating the timing of movement (Reddy and Potts, 1999; Müller, 2003). Australia contains many examples of reworking of major crustal structures in long-lived cratons (e.g. Dieren et al., 2005; Dutch et al., 2008; Williams and Betts, 2009; Stewart and Betts, 2010; Fraser et al., 2012; Glorie et al., 2017), such as those in the Gawler Craton of South Australia (Fig. 1). Shear zones in the Gawler Craton underwent extensive reworking in response to intracontinental stresses (e.g. Betts and Giles, 2006; Hand et al., 2007). Chronological data within the Gawler Craton related to tectonism and movement of major structures is dominated by monazite U–Pb (Dutch et al., 2008, 2010; Payne et al., 2008), muscovite and biotite $^{40}\text{Ar}/^{39}\text{Ar}$ (Swain et al., 2005; Fraser and Lyons, 2006; Forbes et al., 2012; Fraser et al., 2012), and apatite fission track studies (Gleadow et al., 2002; Hall et al., 2016). However, recent advancements in the

* Corresponding author.

E-mail address: james.hall@adelaide.edu.au (J.W. Hall).

Peer-review under responsibility of China University of Geosciences (Beijing).

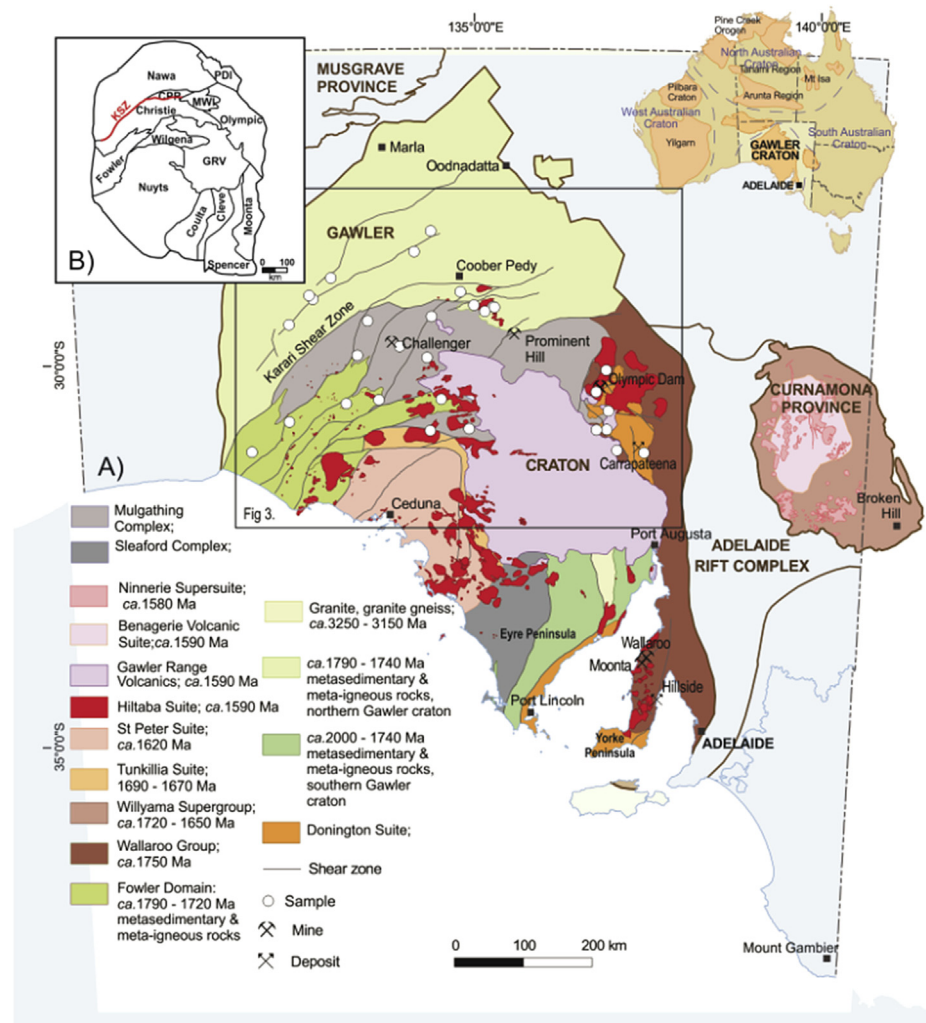


Figure 1. (A) Simplified geological map of the Gawler Craton, indicating the locations of all apatite U–Pb samples (including samples from Hall et al., submitted), and major mineral deposits. Inset (B) illustrating the boundaries of all the domains within the Gawler Craton. Abbreviations are: PDI—Peake and Denison Inliers; CPR—Coober Pedy Ridge; MWI—Mt. Woods Inlier; KSZ—Karari Shear Zone; GRV—Gawler Range Volcanics. Modified from Reid et al. (2014).

U–Pb dating of apatite (Chew et al., 2011, 2014), allow the use of a new radiometric clock to calculate cooling ages through a closure temperature of ~350–550 °C (Chew and Spikings, 2015). This is an emerging method which can be applied in many different settings, such as the thermochronology of mineral deposits (e.g. Liu et al., 2014), or constraints on rift formation (e.g. Zhang et al., 2017) or to date mafic rocks (e.g. Pochon et al., 2016). Here, we have applied the apatite U–Pb radiometric clock to enhance our understanding of the buried Gawler Craton terranes and their Proterozoic thermal evolution.

We present the first apatite U–Pb dataset from within the Gawler Craton, to uncover the spatial distribution of cooling events in relation to various tectonic events throughout the Palaeo-Mesoproterozoic. This dataset reveals post-orogenic cooling from at least four different orogenic events, over a ~1 Ga time span from ~2.3 Ga to 1.3 Ga. The apatite U–Pb data are subsequently compared to pre-existing muscovite, biotite and hornblende $^{40}\text{Ar}/^{39}\text{Ar}$ data from the Gawler Craton (Foster and Ehlers, 1998; Tomkins and Mavrogenes, 2002; Budd and Fraser, 2004; Tomkins et al., 2004; Fraser and Lyons, 2006; Forbes et al., 2012; Fraser et al., 2012; Reid et al., 2017). These two datasets reveal ages that are well correlated, and therefore have been combined to produce a

Mesoproterozoic middle crustal cooling map that illustrates the spatial extent for the timing of the ~550–350 °C cooling history across the northern Gawler Craton at the present-day surface. In addition, they provide valuable information concerning the timing of reactivation of major crustal structures as both datasets preserve differential cooling across these major structures.

2. Geological setting

The Gawler Craton is an Archaean–Mesoproterozoic craton that occupies most of South Australia. There are two major periods of craton growth, firstly, during the late Archaean (~2500–2400 Ma) and then from ~2000 Ma to 1550 Ma (Daly et al., 1998; Hand et al., 2007). These two periods of craton growth are separated by an interval of quiescence with no recorded geological activity (Fig. 2). The Gawler Craton can be subdivided into a number of different domains based on magnetic surveys (Fairclough et al., 2003). The northern Gawler Craton consists of the Coober Pedy Ridge, Mount Woods Inlier, Nawa, Christie, Fowler, Wilgena, Coulta, Nuyts, and Olympic domains (Fig. 1). The rocks that make up these domains are discussed below and the associated periods of craton development are summarised in Fig. 2.

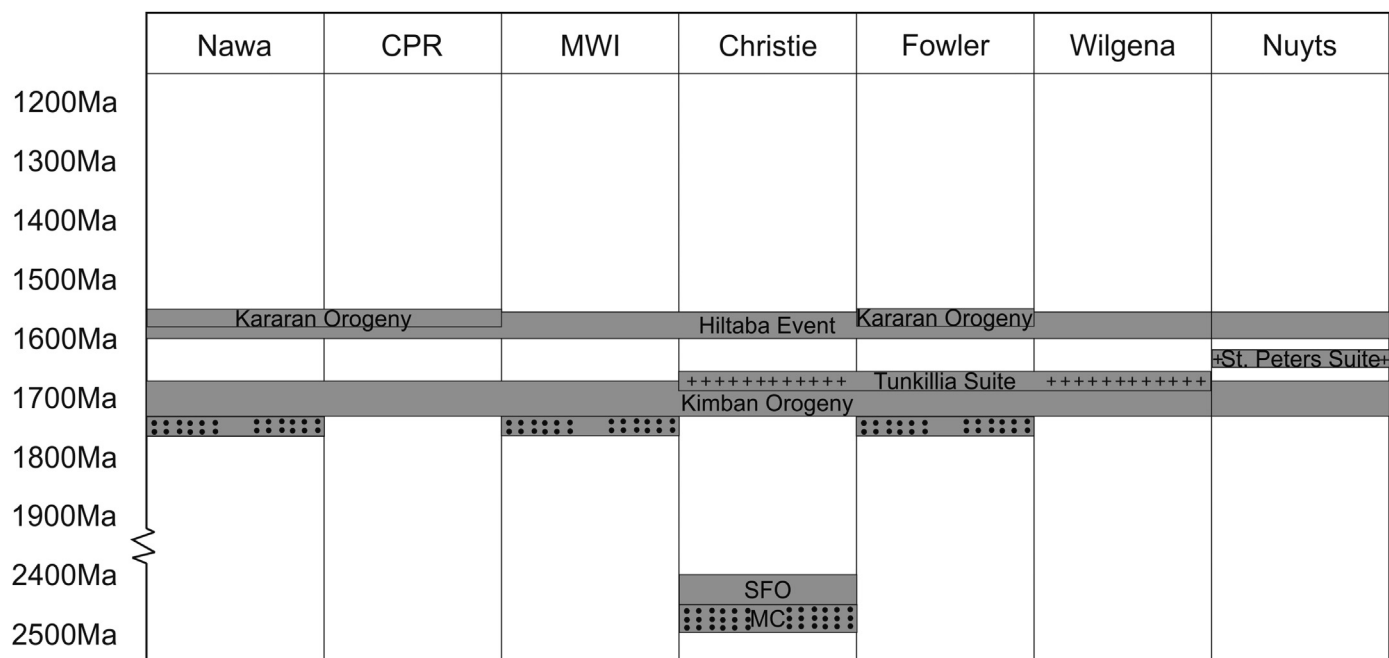


Figure 2. Simplified time-space plot illustrating the different geological events within the different domains of the Gawler Craton through time. The domains are ordered from north, on the left, to south, on the right. Abbreviations are: CPR—Coober Pedy Ridge; MWI—Mt. Woods Inlier; SFO—Sleaford Orogeny; MC—Mulgathering Complex.

The Sleaford and Mulgathering complexes form the Archaean nucleus of the Gawler Craton (Fig. 1). They both include ~2560–2480 Ma volcanosedimentary rocks and felsic to intermediate intrusions (Cowley and Fanning, 1991; Jagodzinski et al., 2009; Reid et al., 2009, 2010, 2014), these complexes are located in the north-west Christie Domain (Mulgathering Complex) and central south Coulta Domain (Sleaford Complex) of the craton. They were subsequently deformed and metamorphosed during the Sleafordian Orogeny at ~2470–2410 Ma (Daly et al., 1998; Fanning et al., 2007; Reid et al., 2014). The Sleafordian Orogeny reached granulite facies and metamorphic conditions of ~850 °C and 5–7 kbar in the central Mulgathering Complex (Halpin and Reid, 2016). The end of the orogeny ushered in a ~400 Ma tectonic hiatus within the Gawler Craton and signalled the end of the first phase of craton growth (Hand et al., 2007).

The second phase of craton growth can be further divided into rift-basin development from ~2000–1690 Ma and magmatism from 1690–1500 Ma (Hand et al., 2007). To the east, deposition of the Hutchison Group (Parker and Lemon, 1982; Fanning et al., 2007; Szpunar et al., 2011), and the emplacement of the Donington Suite at ~1850 Ma (both located within the Olympic Domain; Fig. 1) initiated the second phase (Fig. 1; Jagodzinski, 2005). Reid et al. (2008) suggested that the Donington Suite was emplaced in an intracontinental back arc basin setting, and was associated with the ~1850–1840 Ma Cornian Orogeny. Further rifting along the eastern margin accommodated the deposition of the Wallaroo Group and its associated magmatism from 1770–1740 Ma, while widespread coeval deposition across the Gawler Craton is represented by the formation of the Price Metasediments, Moonabie Formation, Mount Woods Inlier Sediments, Peake Metamorphics, and metasediments within the Fowler and Nawa domains (Fig. 1; Fanning et al., 1988; Parker et al., 1993; Oliver and Fanning, 1997; Daly et al., 1998; Cowley et al., 2003; Jagodzinski, 2005; Hand et al., 2007).

The craton-wide 1730–1690 Ma, high temperature, deformation event known as the Kimban Orogeny, caused magmatism and transpressional deformation, particularly in the southern Gawler

Craton (Hand et al., 2007). The peak metamorphic conditions ranged from 800–900 °C and 7–10 kbar (Parker et al., 1993; Payne et al., 2008), with the highest metamorphic conditions recorded in the far west of the craton, in the Fowler Domain. Stresses related to the Kimban Orogeny were accommodated by movement along the Karari Shear Zone and Tallacootra Shear Zone at ~1680 ± 37 Ma in the Fowler Domain (Swain et al., 2005; Stewart et al., 2009).

Following the start of the Kimban Orogeny, the 1690–1670 Ma I-type Tunkillia Suite was emplaced in the central Gawler Craton (Ferris and Schwarz, 2004). In the southwest Gawler Craton, the St. Peter Suite and co-magmatic Nuyts volcanics were emplaced at ~1620 Ma forming the Nuyts Domain (Flint et al., 1990; Rankin et al., 1990; Budd et al., 2001; Hand et al., 2007). This was followed by the ~1590–1570 Ma Hiltaba event that emplaced the Hiltaba Granite and co-magmatic Gawler Range Volcanics (Fig. 1; Giles, 1988; Creaser and White, 1991; Creaser, 1996; Daly et al., 1998; Budd et al., 2001; Skirrow et al., 2002). This event represents one of the largest felsic volcanic systems in the world (Allen et al., 2008) and is associated with the formation of the world class Olympic Dam Cu–Au–U deposit (e.g. McPhie et al., 2011; Ehrig et al., 2012). In addition, the Hiltaba event was associated with deformation around the Gawler Craton, with northwest-southeast compression and metamorphism in the Mount Woods Inlier. The metamorphic conditions reached temperatures of 750 °C at ~4.7 kbar during peak metamorphism (Forbes et al., 2011). Immediately following this metamorphism, the Mt. Woods Inlier underwent exhumation that has been interpreted to be caused by arrival of a mantle plume at the nearby subduction zone which resulted in compression along the Southern Overthrust in the Mount Woods Inlier (Fig. 1; Betts et al., 2009; Forbes et al., 2012).

The ~1590–1560 Ma Kararan Orogeny is the youngest Proterozoic orogenic event recorded within the Gawler Craton, which deformed and metamorphosed the northeast of the craton, including the Karari Shear Zone (Fig. 3; Rankin et al., 1989; Hand et al., 2007; Fraser et al., 2012). The south western Fowler Domain records peak metamorphic conditions of 800 °C and 10 kbar resulting from this orogeny (Teasdale, 1997; Fanning et al.,

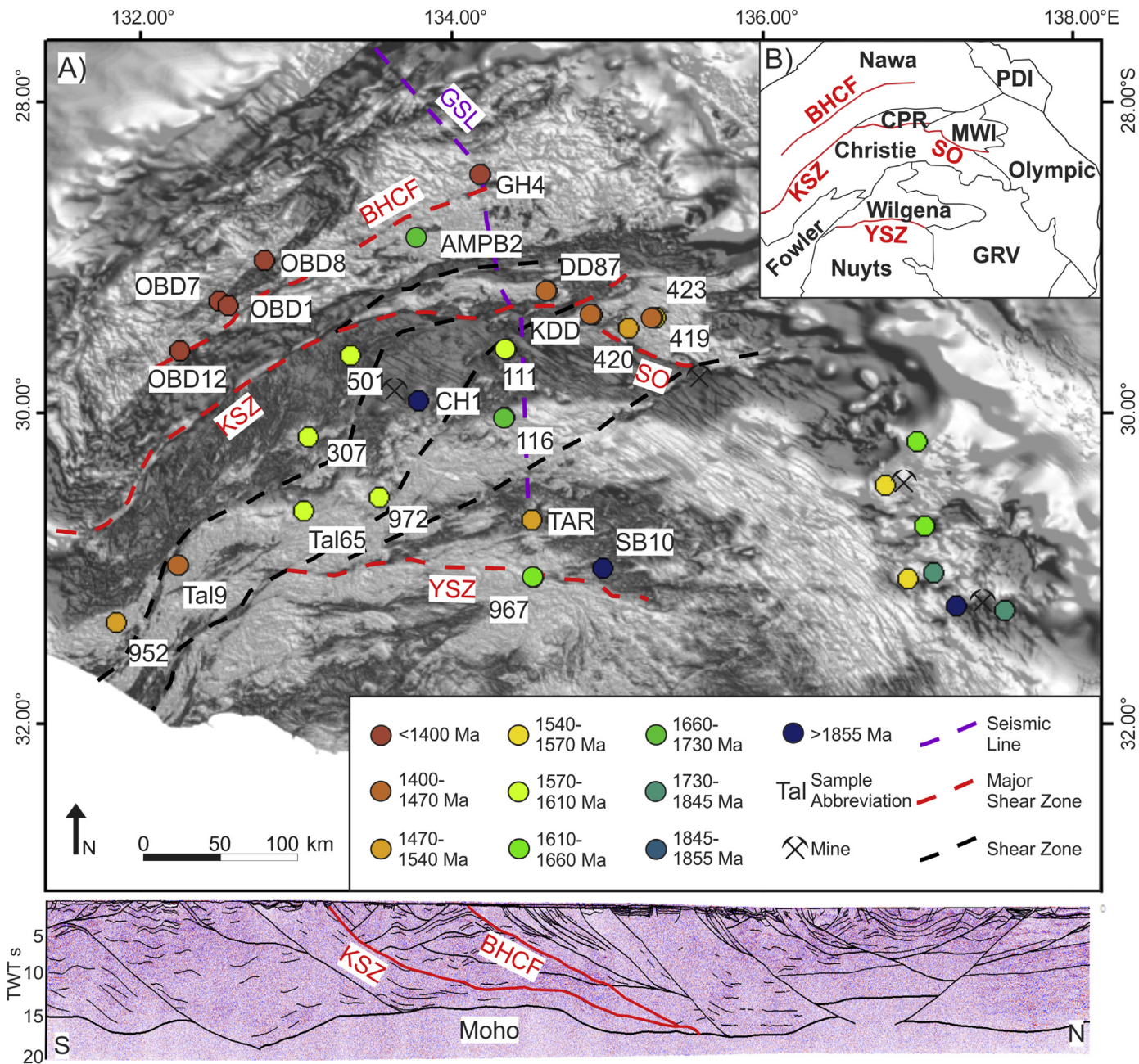


Figure 3. Total Magnetic Intensity (TMI) map of the northern Gawler Craton which reveals shear zones, major mineral mines, the GOMA seismic line, and sample locations (including samples from Hall et al., submitted) and weighted mean ages. GOMA seismic line adapted from Korsch et al. (2010). Abbreviations are: GSL—GOMA seismic line; BHCF—Box Hole Creek Fault; KSZ—Karari Shear Zone; SO—Southern Overthrust; YSZ—Yerda Shear Zone. OBD12—2131385 from drill hole OBD 12; OBD7—2131379 from drill hole OBD 7; OBD1—2131386 from drill hole OBD 01; OBD8—2131380 from drill hole OBD 8; AMPB2—2131373 from drill hole AM/PB 2; GH4—2131374 from drill hole GOMA DH4; DD87—2131367 from drill hole DD87LR 3; KDD—2131371 from drill hole KDD 005; 420—1039420; 423—1039423; 419—1039419; 307—0307; 501—0501; CH1—2131395 from drill hole CH 1; Wall1—650666 from drill hole Wallira 1; 111—2016111; 952—2017967; Tal9—1472758 from drill hole Tal 9; Tal65—1472763 from drill hole Tal 65; 972—2017972; 116—2016116; 967—2017967; SB10—SB12-10. Inset (B) shows the boundaries of the domains within the northern Gawler Craton. Abbreviations are: PDI—Peake and Denison Inliers; BHCF—Box Hole Creek Fault; CPR—Coober Pedy Ridge; MWI—Mt. Woods Inlier; KSZ—Karari Shear Zone; SO—Southern Overthrust; GRV—Gawler Range Volcanics; YSZ—Yerda Shear Zone.

2007), while Fraser et al. (2012) suggested that up to 10 km of exhumation of the Nawa Domain occurred along the Karari Shear Zone during this orogenic event. Both the Yerda Shear Zone and the Coorabie Shear Zone, in the Wilgena and Fowler Domains (Fig. 1), recorded movement at ~1500 Ma following the Kararan Orogeny (McLean and Betts, 2003; Swain et al., 2005). A final period of movement along the Karari Shear zone is recorded at ~1450 Ma and is interpreted to be sinistral strike-slip movement (Fraser and Lyons, 2006; Fraser et al., 2012), whereas coeval deformation on

the Tallacootra Shear Zone is interpreted as forming a large dextral positive flower structure (Stewart et al., 2009).

3. Methodology

All samples were collected from granitoids, either drill core (where the basement was buried), or from exposed rock outcrop. Samples were collected with the intention of an even coverage across major structures (such as the Karari Shear Zone) throughout

the major domains that constitute the northern Gawler Craton. The sampling strategy was therefore aimed at observing the cooling history of the northern Gawler Craton within each domain and across the major structures (Table 1).

Because all sampled rocks were either igneous rocks, or metamorphic rocks that experienced temperatures above ~ 550 °C, apatite U–Pb dating preserves the timing that apatite cooled below its closure temperature of ~ 550 – 350 °C (Chew and Spikings, 2015). Samples were crushed and separated using conventional crushing and separating techniques. Apatites were handpicked, mounted in epoxy resin, and then ground and polished to reveal internal crystal surfaces. Uranium and lead data collection on the Laser-Ablation Inductively-Coupled-Plasma Mass-Spectrometer (LA-ICP-MS) was performed at Adelaide Microscopy, The University of Adelaide. Measured masses were: ^{238}U , ^{232}Th , ^{208}Pb , ^{207}Pb , ^{206}Pb , ^{204}Pb , ^{91}Zr , ^{44}Ca , ^{43}Ca , ^{35}Cl , and ^{29}Si . All samples were ablated for 30 s on a 30 μm spot at $\sim 5 \text{ J/cm}^2$, after a 30 s laser warm up period and a 20 s dwell in between samples. All samples were ablated with a New Wave 213 laser. Samples SB12–10, 12, 13 and TAR were analysed on an Agilent 7900 quadrupole mass-spectrometer, while all remaining samples analysed on the previously used Agilent 7500 quadrupole mass-spectrometer. Madagascar apatite (474.25 ± 0.41 Ma, $n = 9$, MSWD = 1.5; Thomson et al., 2012) was used as the primary standard, with Durango apatite (31.44 ± 0.18 Ma; McDowell et al., 2005) and Mt. McClure apatite (518 ± 11 Ma; Thomson et al., 2012) used as secondary standards. We obtained a weighted mean ^{206}Pb – ^{238}U age of 473.4 ± 2.0 Ma ($n = 227$, MSWD = 0.76) for Madagascar apatite, and ^{207}Pb corrected weighted mean ^{206}Pb – ^{238}U ages of 32.08 ± 0.74 Ma ($n = 90$, MSWD = 0.79) for Durango and 529.1 ± 7.2 Ma ($n = 57$, MSWD = 1.6) for Mt. McClure (Fig. 4). All data reduction was completed on Iolite software (Paton et al., 2011) using the data reduction scheme VizualAge_UcomPbline, following the method outlined by Chew et al. (2011, 2014). Common Pb was corrected for using the ^{207}Pb correction (Chew et al., 2014) based on the initial measured ^{207}Pb / ^{206}Pb ratio for individual samples. This is calculated using a Concordia line (referred to as a common Pb line) through the individual analyses on a Tera-Wasserburg plot. Analyses that contained strongly zoned elemental signals or large uncertainties, often due to low ^{238}U (<2 ppm), were removed during

data reduction. Few additional individual outliers, which plotted away from the corresponding common Pb line in Tera-Wasserburg plots, were also removed. Similar methods for data treatment based on the same criteria are outlined in Zattin et al. (2012) and Mark et al. (2016). Concordia and weighted mean plots were created using Isoplot 4.15 (Ludwig, 1999, 2012).

4. Results

All apatite U–Pb data are reported in Table 2 and Fig. 5.

4.1. Nawa domain

Sample 2131385 is a paragneiss that was collected from drill hole OBD 12. It displays a ^{207}Pb corrected weighted mean ^{206}Pb – ^{238}U age of 1289 ± 32 Ma with a MSWD of 1.3 from an average common Pb line with a lower intercept of 1284 ± 93 Ma (MSWD = 3.2; Fig. 5A).

A ^{207}Pb corrected weighted mean ^{206}Pb – ^{238}U age of 1382 ± 13 Ma was recorded for sample 2131379 (a granite collected down drill hole OBD 7), with a MSWD of 1.3. The accompanying Tera-Wasserburg plot revealed a common Pb line lower intercept of 1382 ± 30 Ma with an MSWD of 1.6 (Fig. 5B).

Sample 2131386 is a paragneiss that was collected from drill hole OBD 01 and is located within 7 km of 2131379. The ^{207}Pb corrected weighted mean ^{206}Pb – ^{238}U age is recorded as 1385 ± 19 Ma (MSWD of 1.02). The lower intercept of the common Pb line was recorded at 1384 ± 25 Ma (MSWD = 1.2; Fig. 5C).

A ^{207}Pb corrected weighted mean ^{206}Pb – ^{238}U age of 1276 ± 31 Ma was obtained for sample 2131380 (a granite from drill hole OBD 8), with a MSWD of 1.5. The accompanying Tera-Wasserburg plot displays a common Pb line lower intercept of 1282 ± 76 Ma (MSWD of 1.9; Fig. 5D).

Sample 2131373 was collected from a paragneiss within drill hole AM/PB 2. This sample failed to produce a reliable common Pb line. The best common-Pb line estimate reveals a lower intercept of 1661 ± 57 Ma (MSWD = 3.3), controlled by three grains outside of a cluster of U–Pb ages (Fig. 5E). The ^{207}Pb corrected weighted mean ^{206}Pb – ^{238}U age 1661 ± 27 Ma produced a MSWD of 2.8. A biotite ^{40}Ar / ^{39}Ar plateau age of 1554 ± 5 Ma from the same drill hole

Table 1

Sample details. Formation ages from Finlay (1993); Daly et al. (1998); Cowley (2005); Payne et al. (2006); Hand et al. (2007); Jagodzinski et al. (2009); Jagodzinski and Reid (2010); Howard et al. (2011a); Howard et al. (2011b); Reid et al. (2014); Reid and Fabris (2015), and Dawson (2016).

Sample No.	Drill hole number	Latitude (°S)	Longitude (°E)	Depth (m)	Region	Rock type	Formation age	Metamorphic age (mineral)
2131385	OBD 12	29.6008065	132.2554548	470–471	Nawa Domain	paragneiss	~ 1740 Ma	~ 1550 Ma (zircon)
2131379	OBD 7	29.2831073	132.5062594	261–262	Nawa Domain	granite	1752 ± 9 Ma	1715 ± 17 Ma (zircon)
2131386	OBD 01	29.310519	132.568165	139–140	Nawa Domain	paragneiss	1752 ± 9 Ma	1715 ± 17 Ma (zircon)
2131380	OBD 8	29.017528	132.8058533	183–184	Nawa Domain	granite	~ 1740 Ma	1458 ± 9 Ma (monazite)
2131373	AM/PB 2	28.8199561	133.8273135	344–345	Nawa Domain	paragneiss	~ 1740 Ma	1555 ± 11 Ma (Monazite)
2131374	GOMA DH4	28.4687532	134.1938652	512–514	Nawa Domain	paragneiss	2462 ± 17 Ma	1523 ± 10 Ma (zircon)
2131367	DD87LR 3	29.2146561	134.619117	93–95	Coober Pedy Ridge	gabbro	~ 1740 Ma	-
2131371	KDD 005	29.3758388	134.9082905	333–336	Coober Pedy Ridge	paragneiss	~ 1740 Ma	1590 ± 10 Ma (monazite)
1039420	-	29.3899993	135.295242	-	Mt. Woods Inlier	granite	1584 ± 18 Ma	-
1039423	-	29.4616	135.145611	-	Mt. Woods Inlier	granite	1584 ± 18 Ma	-
1039419	-	29.396233	135.313564	-	Mt. Woods Inlier	granite	1584 ± 18 Ma	-
0307	-	30.15667473	133.088121117	-	Christie Domain	granite	1695 ± 6 Ma	-
0501	-	29.63513888	133.3580277	-	Christie Domain	granite	2493 ± 6 Ma	2565 Ma (Zircon)
2131395	CH 1	29.9253457	133.7903421	68–80	Christie Domain	granite	2440 ± 20 Ma	-
2016111	-	29.5934	134.355	-	Christie Domain	granite	tonalite	-
2017952	-	31.3528	131.8547	-	Fowler Domain	gabbro	granite	1718 ± 15 Ma (zircon)
1472758	Tal 9	30.9871284	132.2473098	21.8–22.5	Fowler Domain	paragneiss	1698 ± 7 Ma	-
1472763	Tal 65	30.6371679	133.0589695	56–59.5	Fowler Domain	gabbronorite	1583 ± 5 Ma	-
2017972	-	30.5509	133.5415	-	Fowler Domain	granite	1692 ± 15 Ma	-
2016116	-	30.0318	134.3451	-	Wilgena Domain	granite	~ 1730 Ma	-
TAR	-	30.689	134.517	-	Wilgena Domain	granite	1587 ± 20 Ma	-
2017967	-	31.0582	134.5313	-	Wilgena Domain	granite	1732 ± 15 Ma	-
SB12-10	-	31.008	134.976	-	Wilgena Domain	granite	2507 ± 3 Ma	-

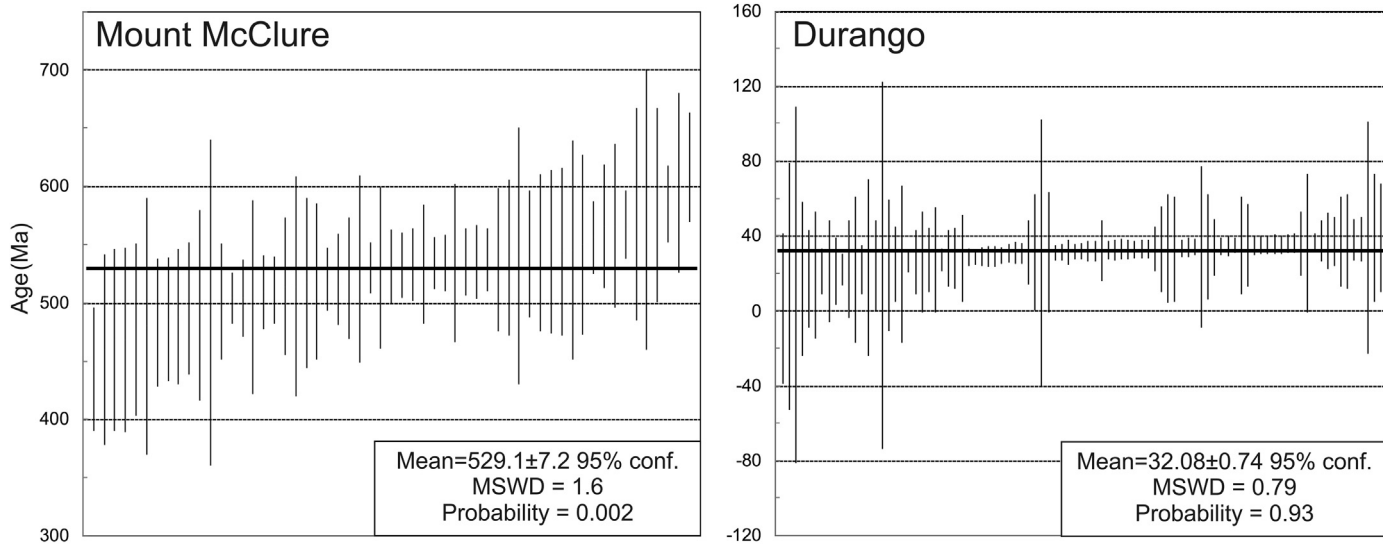


Figure 4. ^{207}Pb corrected weighted mean ^{206}Pb - ^{238}U age for secondary standards Mount McClure (518 ± 11 Ma; Thomson et al., 2012) and Durango (31.44 ± 0.18 Ma; McDowell et al., 2005). Weighted mean is ordered by age.

(Fraser et al., 2012) suggests that the sample had cooled to temperatures of ~ 300 °C by this time.

Only five grains were analysed from sample 2131374 (a paragneiss from drill hole GOMA DH4), however, an adequate common Pb line was produced, with a lower intercept of 1334 ± 160 Ma with an MSWD of 0.48. An associated ^{207}Pb corrected weighted mean ^{206}Pb - ^{238}U age of 1331 ± 50 Ma was produced from this common Pb line, with an MSWD of 0.17 (Fig. 5F).

In summary, the five reliable samples within the Nawa Domain preserve U-Pb ages between 1276 ± 31 Ma and 1385 ± 19 Ma, which suggests cooling through ~ 550 – 350 °C across the terrane at ~ 1400 – 1300 Ma. The final sample preserves a poorly constrained older age of 1661 ± 57 Ma which, when combined with a biotite $^{40}\text{Ar}/^{39}\text{Ar}$ from Fraser et al. (2012) indicates that this sample cooled

below ~ 300 °C over 150 Ma before the other five samples within the Nawa Domain.

4.2. Coober Pedy Ridge & Mt. Woods Inlier

Sample 2131367, which was collected from a gabbro down drill hole DD87LR 3, produced a reliable common Pb line with a lower intercept of 1402 ± 33 and a MSWD of 1.4. This common-Pb line was used in the calculation of the ^{207}Pb corrected weighted mean ^{206}Pb - ^{238}U age of 1413 ± 17 Ma (MSWD = 1.03; Fig. 5G). This age is slightly younger than the recorded biotite $^{40}\text{Ar}/^{39}\text{Ar}$ pseudo-plateau age of 1476 ± 5 Ma from the same drill hole (Fraser et al., 2012), which indicates this sample underwent cooling at ~ 1.4 Ga.

Table 2
Apatite U-Pb data, where n = number of analyses, and $^{39}\text{Ar}/^{40}\text{Ar}$ age = $^{39}\text{Ar}/^{40}\text{Ar}$ age of a sample nearby or within the same drill hole from Budd and Fraser (2004); Fraser and Lyons (2006); Forbes et al. (2012); and Fraser et al. (2012).

Sample	Drill hole number	n	Concordia intercept	MSWD	$^{207}\text{Pb}/^{206}\text{Pb}$ intercept	^{207}Pb corrected ^{206}Pb - ^{238}U age	MSWD	Probability	$^{39}\text{Ar}/^{40}\text{Ar}$ age (mineral)
2131385	OBD 12	15	1284 ± 93 Ma	3.2	0.7232	1289 ± 32 Ma	1.3	0.22	-
2131379	OBD 7	39	1382 ± 30 Ma	1.6	0.7867	1382 ± 13 Ma	1.3	0.086	-
2131386	OBD 01	27	1384 ± 25 Ma	1.2	0.7829	1385 ± 19 Ma	1.02	0.43	-
2131380	OBD 8	13	1282 ± 76 Ma	1.9	0.7506	1276 ± 31 Ma	1.5	0.11	-
2131373	AM/PB 2	38	1661 ± 67 Ma	3.3	0.8801	1661 ± 27 Ma	2.8	0.00	1554 ± 5 Ma (Biotite)
2131374	GOMA DH4	5	1334 ± 160 Ma	0.48	0.7017	1331 ± 50 Ma	0.17	0.95	-
2131367	DD87LR 3	38	1402 ± 33 Ma	1.4	0.7461	1413 ± 17 Ma	1.03	0.42	1476 ± 5 Ma (Biotite)
2131371	KDD 005	21	1449 ± 91 Ma	1.8	0.8617	1429 ± 29 Ma	1.15	0.29	-
1039420	-	9	1397 ± 130 Ma	2.2	0.401	1404 ± 38 Ma	1.2	0.28	-
1039423	-	13	1469 ± 45 Ma	0.86	0.7349	1472 ± 27 Ma	0.64	0.81	1529 ± 10 Ma (Biotite)
1039419	-	30	1532 ± 66 Ma	1.6	1.0681	1540 ± 26 Ma	0.93	0.58	-
0307	-	22	1561 ± 64 Ma	1.6	0.8306	1581 ± 36 Ma	0.8	0.73	-
0501	-	5	1520 ± 170 Ma	0.071	0.8088	1597 ± 100 Ma	0.28	0.89	-
2131395	CH 1	11	1994 ± 96 Ma	2.7	1.3369	1983 ± 38 Ma	1.19	0.29	-
2016111	-	12	1599 ± 64 Ma	1.5	0.7689	1592 ± 65 Ma	1.4	0.19	-
2017952	-	33	1526 ± 80 Ma	1.3	0.7887	1533 ± 41 Ma	1.03	0.42	-
1472758	Tal 9	37	1436 ± 78 Ma	1.8	0.8552	1442 ± 37 Ma	1.3	0.11	1441 ± 10 Ma (Biotite)
1472763	Tal 65	24	1572 ± 68 Ma	0.71	0.7199	1588 ± 30 Ma	0.96	0.52	-
2017972	-	23	1596 ± 67 Ma	1.5	0.7368	1602 ± 50 Ma	1.18	0.25	-
2016116	-	20	1661 ± 77 Ma	1.2	0.7441	1670 ± 45 Ma	1.15	0.29	-
TAR	-	34	1531 ± 33 Ma	1.8	0.8158	1539 ± 14 Ma	1.16	0.25	1582 ± 5 Ma (Hornblende)
2017967	-	35	1616 ± 72 Ma	2.0	1.1463	1627 ± 33 Ma	1.6	0.013	1586 ± 11 Ma (Biotite)
SB12-10	-	30	2300 ± 53 Ma	1.8	0.8077	2299 ± 19 Ma	1.02	0.43	-

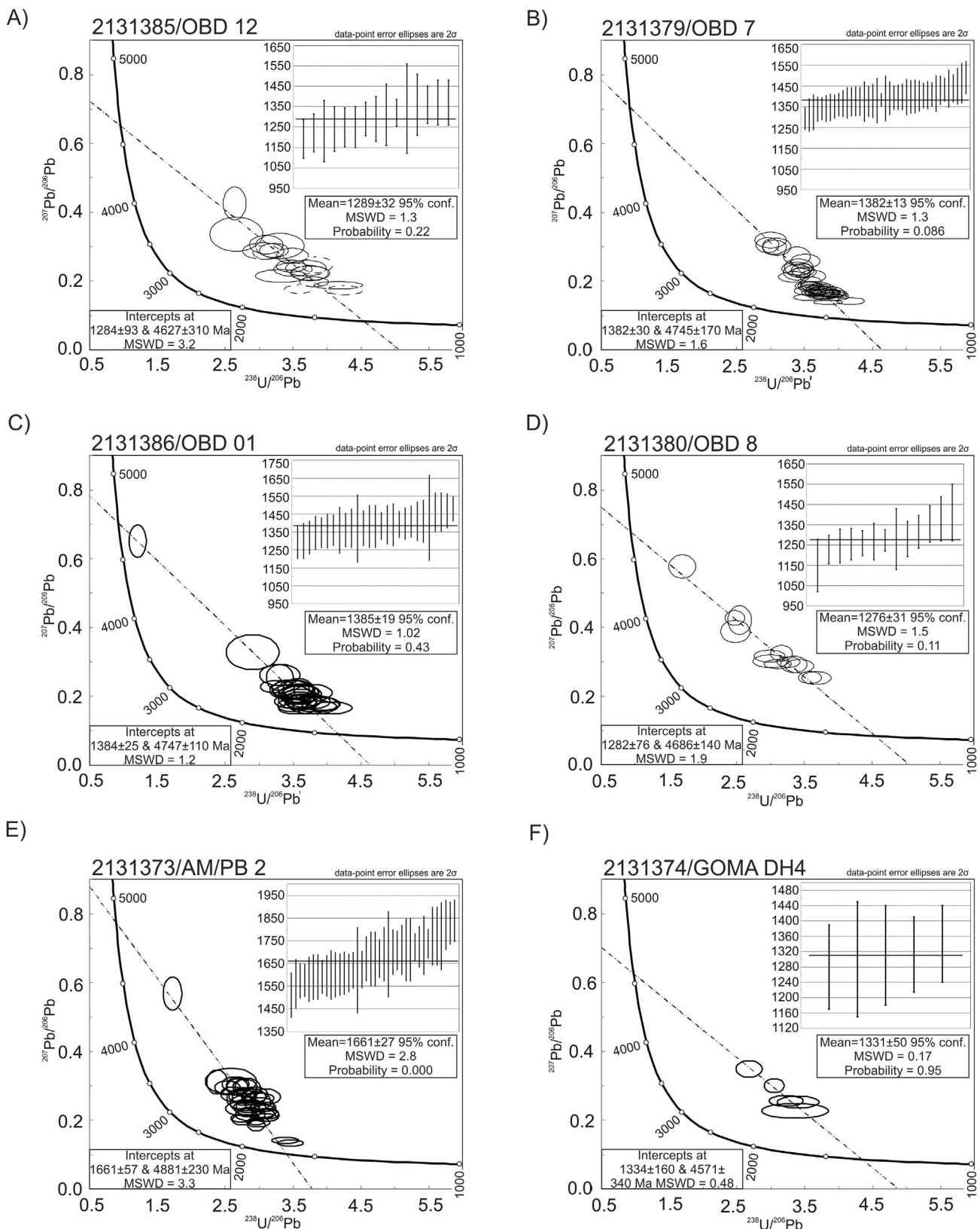


Figure 5. Tera-Wasserburg concordia plots and associated ^{207}Pb corrected weighted mean plots for all samples. Data points with dashed lines were included in ^{207}Pb correction but were later excluded from the weighted mean plots. Tera-Wasserburg plots that contain dashed data-symbols indicate these analyses were used in the ^{207}Pb correction but have been removed from the ^{207}Pb corrected ^{206}Pb – ^{238}U weighted mean plot as they were found to only hold information on the common Pb line but little accurate information in the weighted mean plots.(Continued).

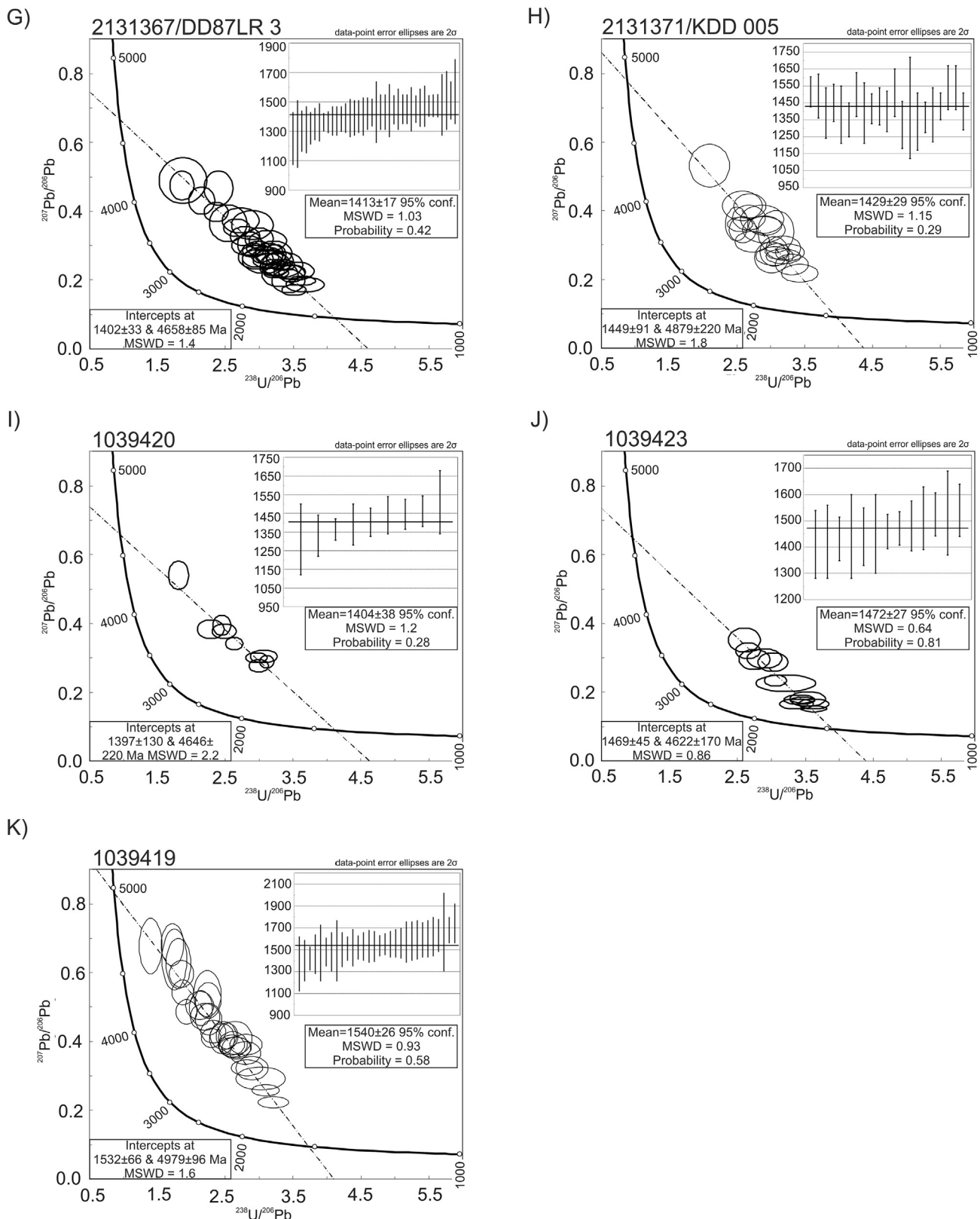


Figure 5. (continued).

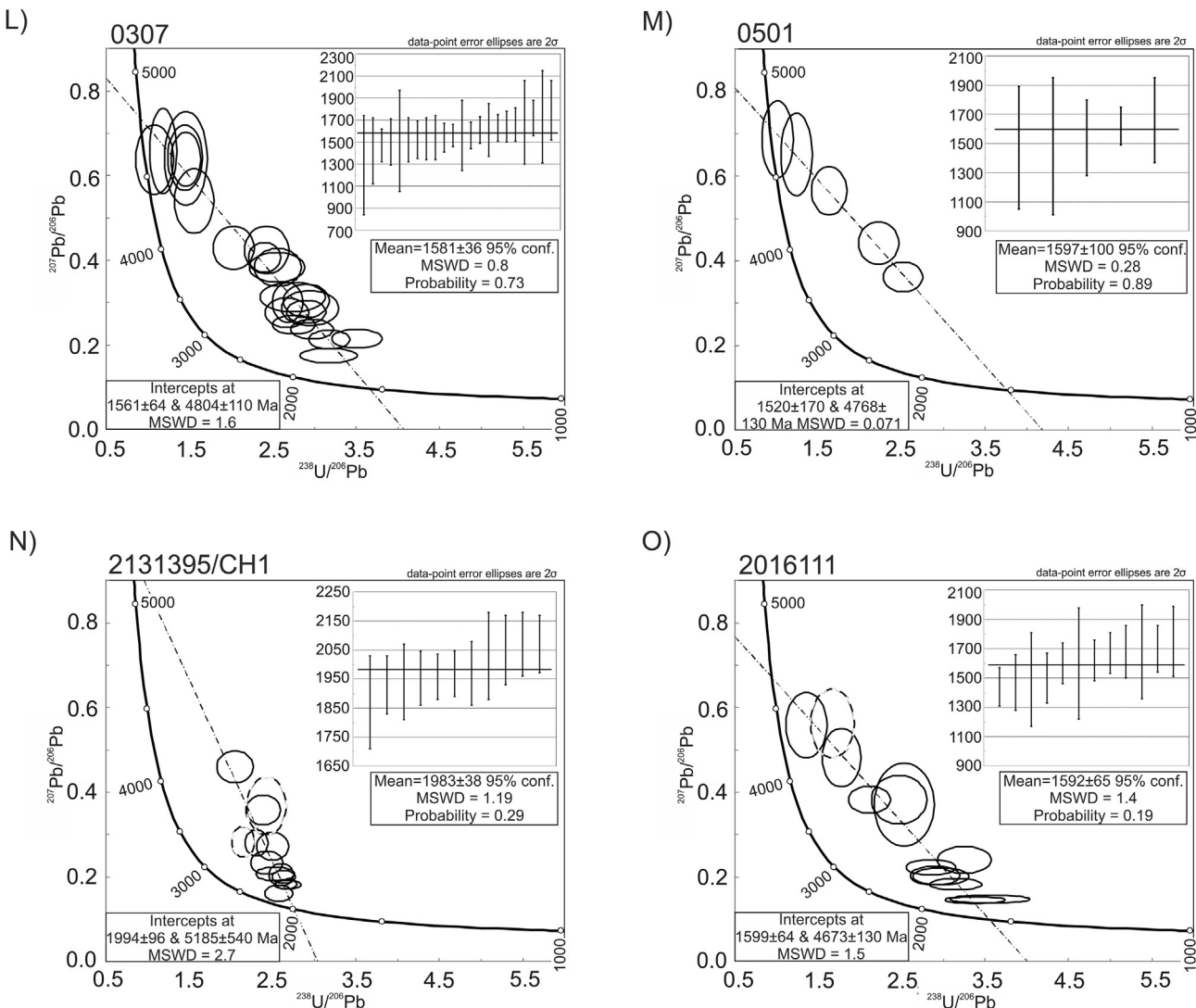


Figure 5. (continued).

A ^{207}Pb corrected weighted mean $^{206}\text{Pb}-^{238}\text{U}$ age of 1429 ± 29 Ma (MSWD of 1.15) was obtained from sample 2131371 (a paragneiss collected from KDD 005). A common Pb line with a lower intercept of 1449 ± 91 Ma (MSWD = 1.8; Fig. 5H) was also calculated from these data.

Sample 1039420 is a granite outcrop sample that recorded a common Pb line lower intercept of 1397 ± 130 Ma with a MSWD of 2.2. The associated ^{207}Pb corrected $^{206}\text{Pb}-^{238}\text{U}$ weighted mean produced an age of 1404 ± 38 Ma with an MSWD of 1.2 (Fig. 5I).

Sample 1039423 is another granite outcrop sample. A ^{207}Pb corrected weighted mean $^{206}\text{Pb}-^{238}\text{U}$ age of 1472 ± 27 Ma (MSWD = 0.64) was observed for this sample. The associated common Pb line yields a lower intercept age of 1469 ± 45 Ma with an MSWD of 0.86 (Fig. 5J). A nearby biotite $^{40}\text{Ar}/^{39}\text{Ar}$ plateau age of 1529 ± 10 Ma (Forbes et al., 2012) is in relatively good agreement with this sample and indicates this region underwent cooling at around 1.5 Ga.

Sample 1039419 was taken from a granite. It produced a ^{207}Pb corrected weighted mean $^{206}\text{Pb}-^{238}\text{U}$ age of 1540 ± 26 Ma (MSWD of 0.93) from a reliable common Pb line, which produced a lower intercept of 1532 ± 66 Ma (MSWD of 1.6; Fig. 5K).

These two domains preserve very similar U–Pb ages which range between 1404 ± 38 Ma and 1540 ± 26 Ma from 5 samples.

4.3. Christie domain

Sample 0307 was taken from a granite outcrop. A reliable common Pb line lower intercept age of 1561 ± 54 Ma (MSWD of 1.6) was recorded in this sample, with a ^{207}Pb corrected weighted mean $^{206}\text{Pb}-^{238}\text{U}$ age of 1581 ± 36 Ma (MSWD of 0.8) produced from the common Pb line (Fig. 5L).

Sample 0501 is an outcropping tonalite. It only produced five reliable dates, yet these dates form a good common Pb line, with a lower intercept of 1520 ± 170 Ma and a MSWD of 0.071. The resultant ^{207}Pb corrected weighted mean revealed a $^{206}\text{Pb}-^{238}\text{U}$ age of 1597 ± 100 Ma with a MSWD of 0.28 (Fig. 5M).

Sample 2131395 was a granite collected from drill hole CH 1. It recorded a ^{207}Pb corrected weighted mean $^{206}\text{Pb}-^{238}\text{U}$ age of 1983 ± 38 Ma (MSWD = 1.19) from a common Pb line with a lower intercept of 1994 ± 96 Ma (MSWD = 2.7; Fig. 5N).

Sample 2016111 is a Hiltaba granite. It preserved a common Pb line with a lower intercept of 1599 ± 64 Ma (MSWD of 1.5). The

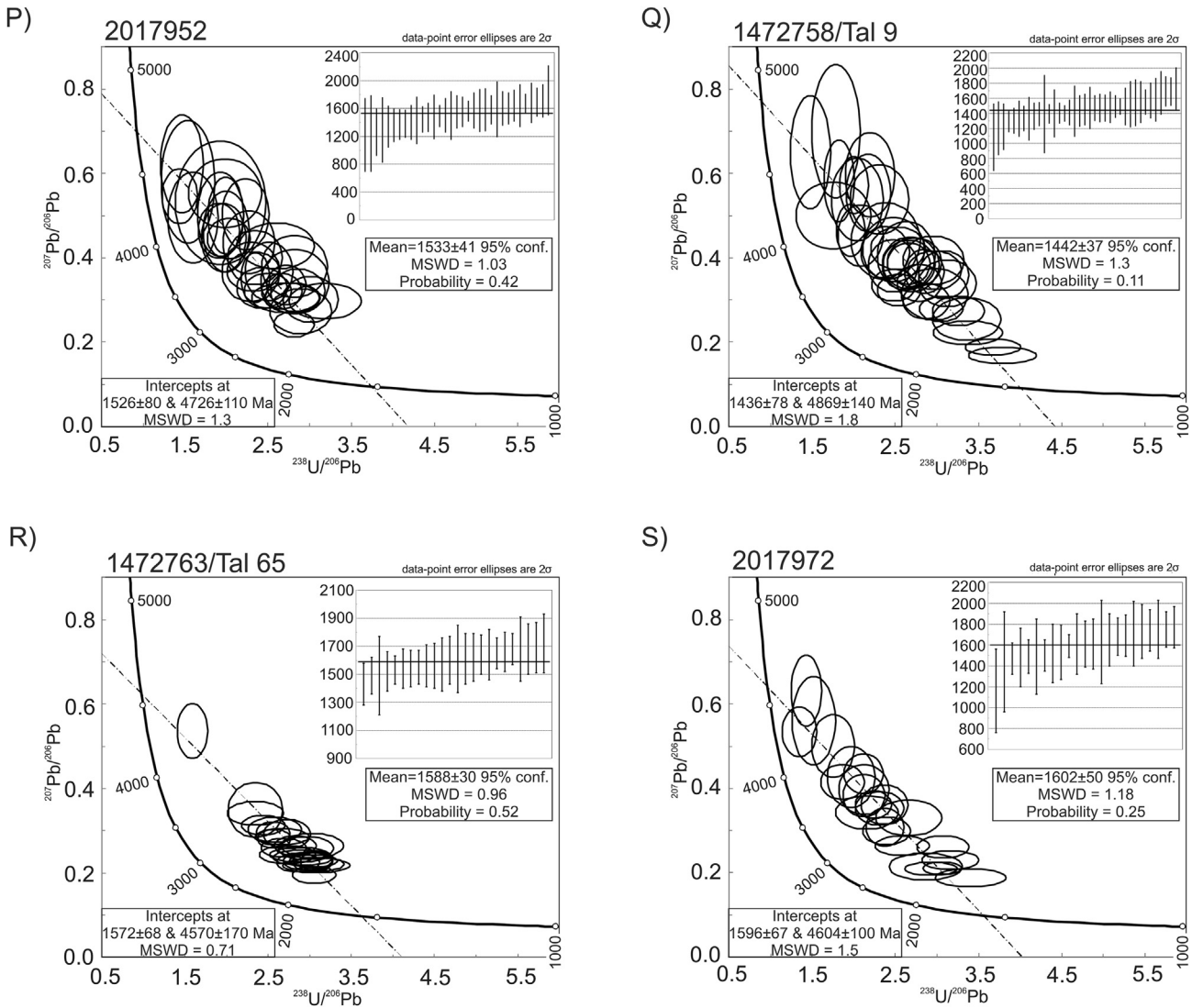


Figure 5. (continued).

calculated ^{207}Pb corrected weighted mean produced a ^{206}Pb – ^{238}U age of 1592 ± 65 Ma with a MSWD of 1.4 (Fig. 5O).

Three of the four samples preserve cooling at ~ 1600 – 1500 Ma, with the other recording cooling at 1983 ± 38 Ma. The ~ 1600 – 1500 Ma samples were from rocks that are thought to have crystallised at around the same time, suggesting that they represent rapid post-crystallisation cooling.

4.4. Fowler domain

A ^{207}Pb corrected weighted mean ^{206}Pb – ^{238}U age of 1533 ± 41 Ma (MSWD = 1.03) was recorded in sample 2017952. This sample also records a common Pb line lower intercept of 1526 ± 80 Ma (MSWD = 1.3; Fig. 5P).

Sample 1472758 (from drill hole Tal 9) produced a reliable common Pb line with a lower intercept of 1436 ± 78 Ma and a MSWD of 1.8. This common Pb line was used to produce the ^{207}Pb corrected weighted mean ^{206}Pb – ^{238}U age of 1442 ± 37 Ma, with a MSWD of 1.3 (Fig. 5Q). A biotite $^{40}\text{Ar}/^{39}\text{Ar}$ sample located 7 km to the south west is in very good agreement with this sample as it records a plateau age of 1441 ± 10 Ma (Fraser and Lyons, 2006).

Sample 1472763 is a gabbronorite collected from drill hole Tal 65. It recorded a ^{207}Pb corrected weighted mean ^{206}Pb – ^{238}U age of 1588 ± 30 Ma with a MSWD of 0.96. The associated common Pb line recorded a lower intercept age of 1572 ± 68 Ma with a MSWD of 0.71 (Fig. 5R).

Sample 2017972 is an outcrop of granite. It records a reliable common Pb line with a lower intercept of 1596 ± 67 Ma (MSWD of 1.5). The ^{207}Pb corrected weighted mean records a ^{206}Pb – ^{238}U age of 1602 ± 50 Ma with a MSWD of 1.18 (Fig. 5S).

The four samples within the Fowler Domain preserve U–Pb ages between 1442 ± 37 Ma and 1602 ± 50 Ma.

4.5. Wilgena & Nuyts domains

Sample 2016116 preserved a ^{207}Pb corrected weighted mean ^{206}Pb – ^{238}U age of 1670 ± 45 Ma with a MSWD of 1.15. The ^{207}Pb correction was calculated on a common Pb line with a lower intercept of 1661 ± 77 Ma (MSWD of 1.2; Fig. 5T).

TAR was collected from a Hiltaba granite. A reliable common Pb line was produced for this sample, with a lower intercept of 1531 ± 33 (MSWD = 1.8). The ^{207}Pb corrected weighted mean plot

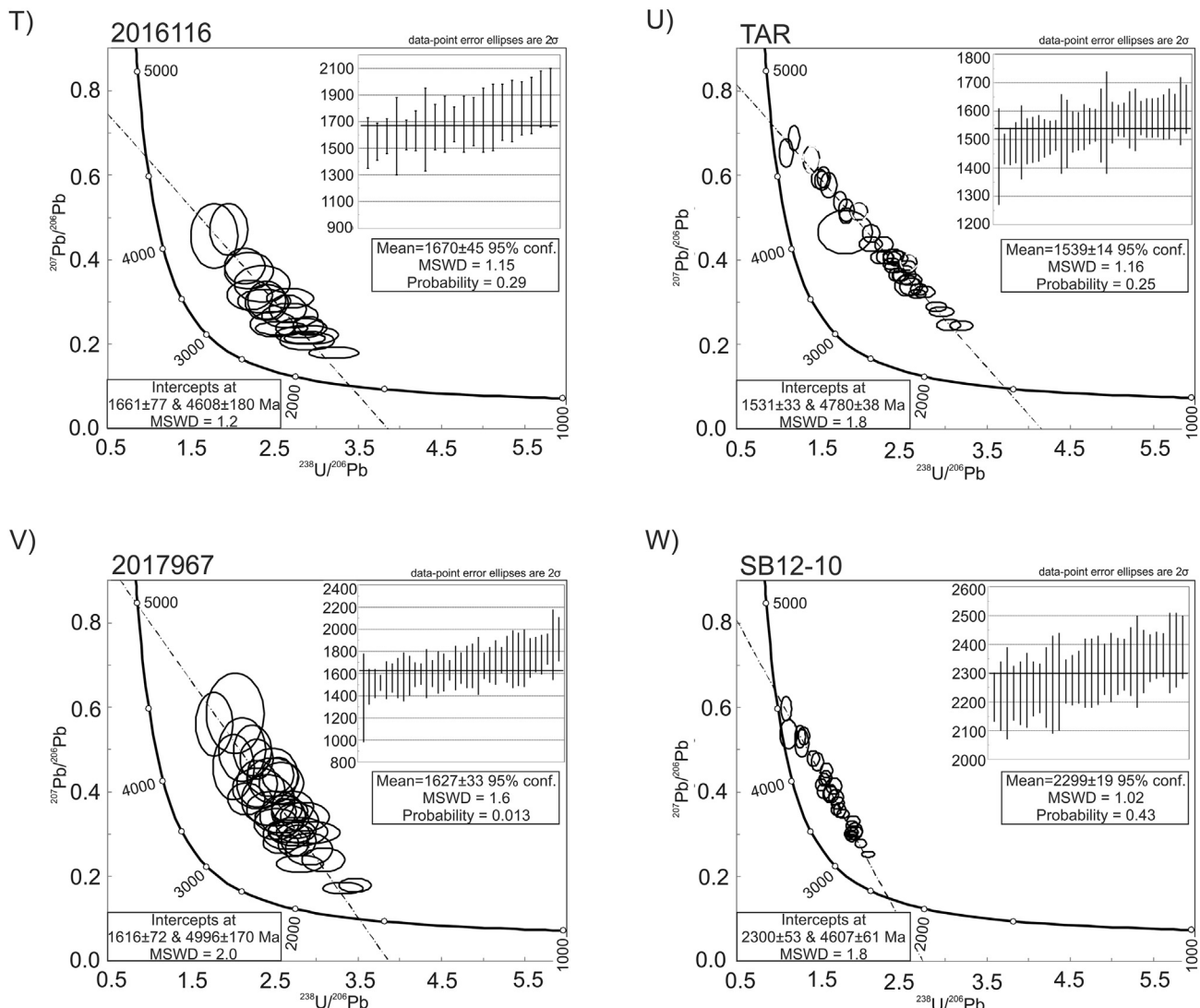


Figure 5. (continued).

produced a ^{206}Pb - ^{238}U age of 1539 ± 14 Ma with a MSWD of 1.16 (Fig. 5U). A hornblende ^{40}Ar / ^{39}Ar sample located 2 km to the south east of TAR preserves a plateau age of 1582 ± 5 Ma (Budd and Fraser, 2004). Given the difference in closure temperatures between ^{40}Ar / ^{39}Ar in hornblende ($\sim 450^\circ\text{C}$; McDougall and Harrison, 1999) and U-Pb in apatite (350°C), it is considered these two ages are part of the same cooling event.

Sample 2017967 is a granite sample. It yielded a ^{207}Pb corrected weighted mean ^{206}Pb - ^{238}U age of 1627 ± 33 Ma (MSWD of 1.6). When plotted on a Tera-Wasserburg plot a common Pb line with a lower intercept of 1616 ± 72 Ma (MSWD of 2.0) was produced (Fig. 5V).

A ^{207}Pb corrected weighted mean ^{206}Pb - ^{238}U age of 2299 ± 19 Ma (MSWD of 1.02) was preserved in sample SB12-10 (a Glenloth Granite sample). The common Pb line lower intercept preserved an age of 2300 ± 53 Ma with a MSWD of 1.8 (Fig. 5W).

In summary, all four samples produced reliable U-Pb ages between 1539 ± 14 Ma and 2299 ± 19 Ma. They preserve three periods of cooling, at 2.3 Ga, 1.6 Ga, and 1.5 Ga, the latter probably reflecting post-magmatic cooling of the Hiltaba granite.

5. Discussion

5.1. Palaeoproterozoic cooling

The oldest recorded apatite U-Pb ages within the northern Gawler Craton occur in the Mulgathang Complex of the Christie and Wilgena domains (Figs. 3 and 6). These >1950 Ma U-Pb ages are interpreted to record cooling of the Mulgathang Complex following the end of the Sleaford Orogeny at ~ 2410 Ma (Hand et al., 2007; Jagodzinski et al., 2009; Reid et al., 2010). Moreover, these U-Pb ages indicate that later orogenic events such as the Kimban Orogeny did not homogeneously reheat the Christie and Wilgena domains to temperatures in excess of $\sim 550^\circ\text{C}$ (Parker et al., 1993; Payne et al., 2008). Similarly, ~ 1.6 - 1.7 Ga U-Pb ages that might reflect cooling after the Kimban Orogeny are only preserved in two samples (SB12-10 and 2131395), from the Christie and Wilgena domains. Despite the widespread deformation of both the Sleaford and Kimban orogenies, they are poorly recorded by the apatite U-Pb data, and are also only sparsely recorded in ^{40}Ar / ^{39}Ar data (Fig. 7; Tomkins and Mavrogenes, 2002; Budd and Fraser, 2004;

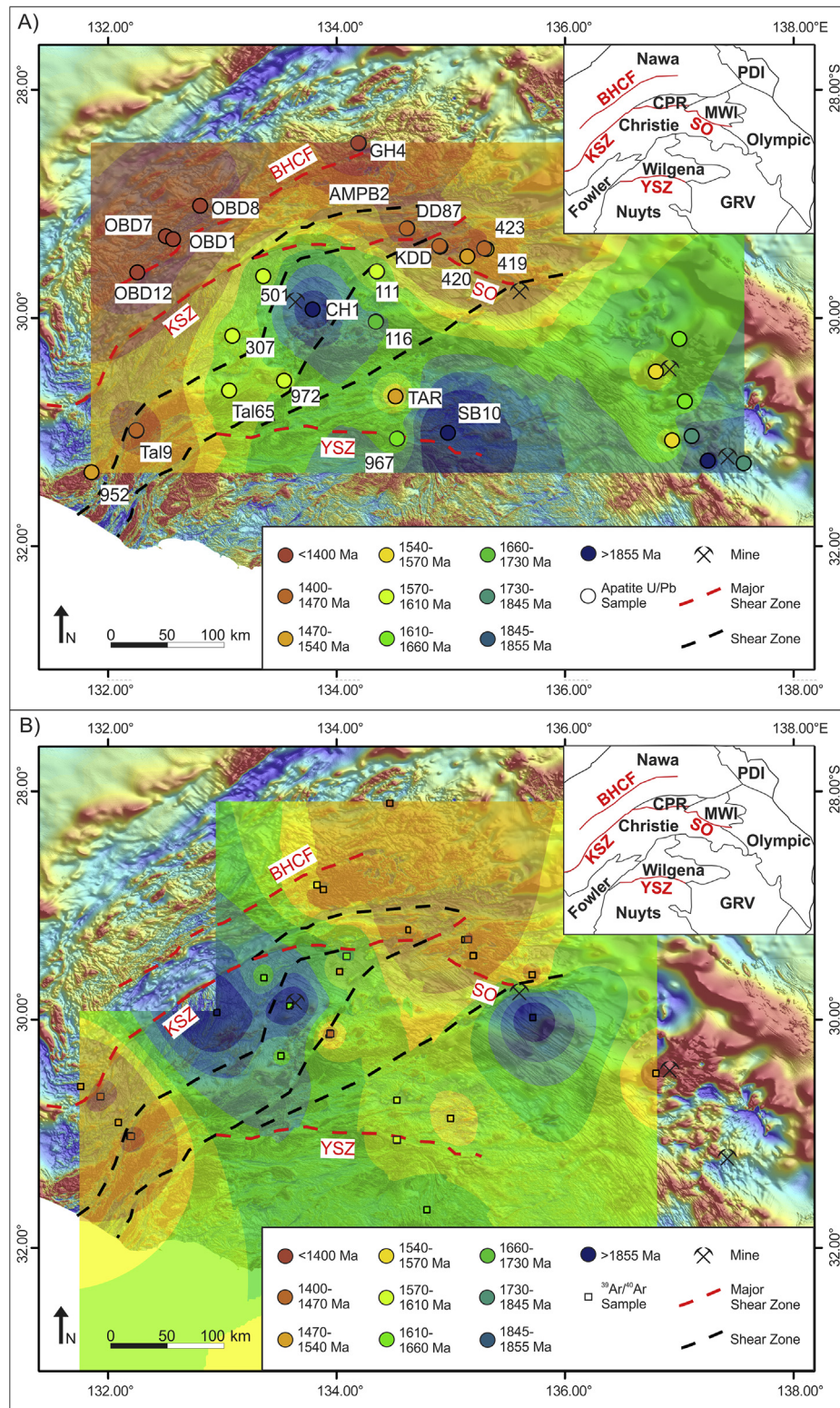


Figure 6. (A) A gridded Inverse Distance Weighting model based on the apatite U–Pb samples, $^{40}\text{Ar}/^{39}\text{Ar}$ samples, shear zones, and major mineral deposits. This map models the ages of cooling in the northern Gawler Craton through the closure temperature of Pb in apatite of $\sim 550\text{--}350^\circ\text{C}$ (Chew and Spikings, 2015). Additional U–Pb apatite data from the Olympic Domain from Hall et al. (submitted). (B) A gridded Inverse Distance Weighting model of mica and hornblende $^{40}\text{Ar}/^{39}\text{Ar}$ ages overlaid on the total magnetic intensity map of the northern Gawler Craton with the same extent and contents as Fig. 6. This map models the ages of cooling through mid-crustal temperatures represented by the closure temperature of Ar in these minerals ($\sim 550\text{--}300^\circ\text{C}$; McDougall and Harrison, 1999; Harrison et al., 2009). $^{40}\text{Ar}/^{39}\text{Ar}$ data from Foster and Ehlers (1998), Tomkins and Mavrogenes (2002), Budd and Fraser (2004), Tomkins et al. (2004), Fraser and Lyons (2006), Fraser et al. (2007), Forbes et al. (2012), Fraser et al. (2012), and Reid et al. (2017). The insets in (A) and (B) show the boundaries of the domains within the northern Gawler Craton. Abbreviations are: PDI—Peake and Denison Inliers; BHCF—Box Hole Creek Fault; CPR—Coober Pedy Ridge; MWI—Mt. Woods Inlier; KSZ—Karari Shear Zone; SO—Southern Overthrust; GRV—Gawler Range Volcanics; YSZ—Yerda Shear Zone.

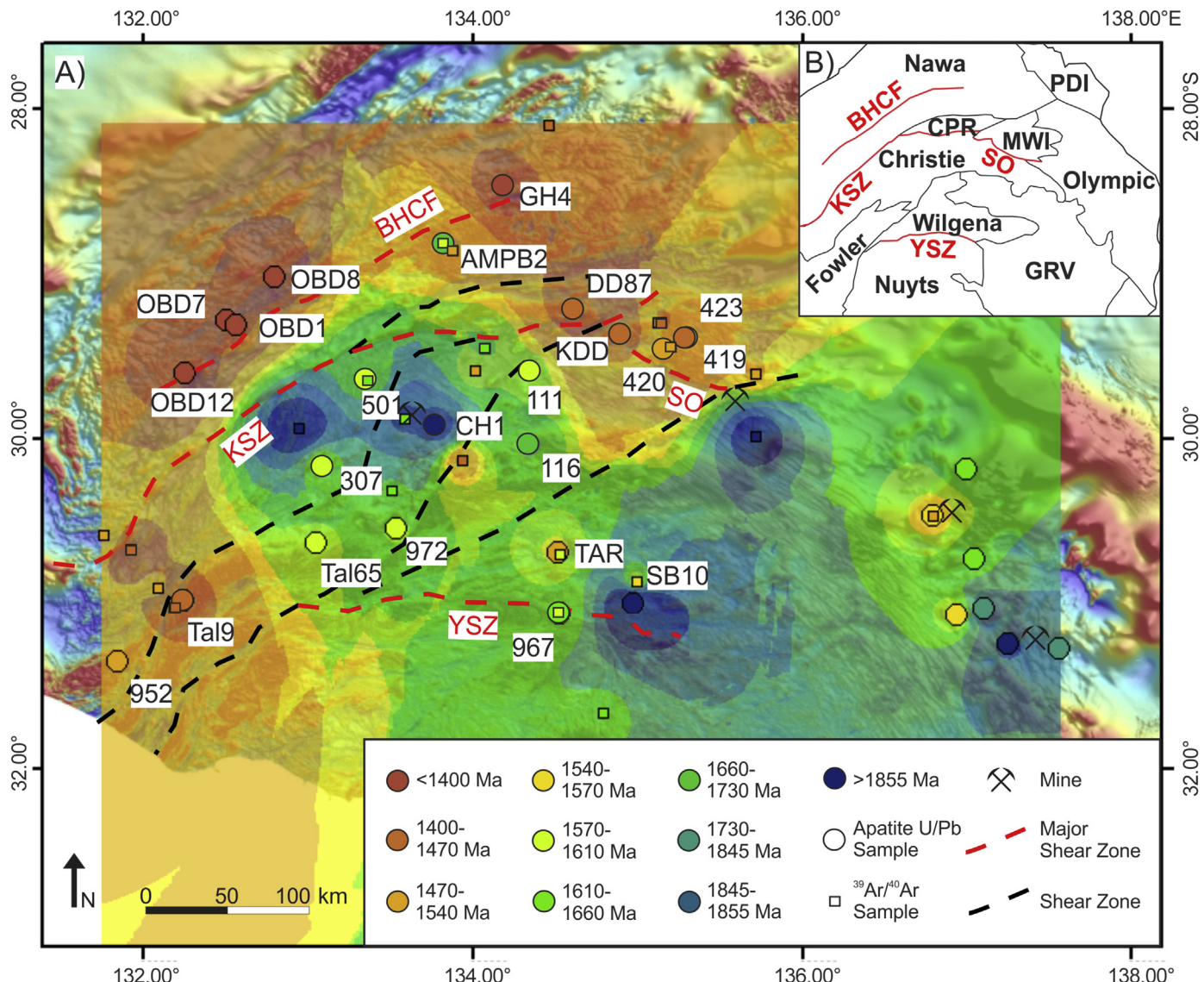


Figure 7. (A) A gridded Inverse Distance Weighting model of the northern Gawler combining all U–Pb apatite ages and mica and hornblende $^{39}\text{Ar}/^{40}\text{Ar}$ ages. Inset (B) reveals the boundaries of the domains within the northern Gawler Craton. Abbreviations are: PDI—Peake and Denison Inliers; BHCF—Box Hole Creek Fault; CPR—Coober Pedy Ridge; MWI—Mt. Woods Inlier; KSZ—Karari Shear Zone; SO—Southern Overthrust; GRV—Gawler Range Volcanics; YSZ—Yerda Shear Zone.

(Tomkins et al., 2004; Fraser et al., 2007) as they are restricted to the Christie Domain. This distribution suggests that the remainder of the Gawler Craton was heated to at least greenschist-facies conditions after the Kimban Orogeny.

To the east, within the Olympic Domain, apatite U–Pb data records cooling following emplacement of the ca. 1850 Ma Donington Suite (Hall et al., submitted). This supports observation that the Kimban Orogeny had minimal effect on the Olympic Domain (Reid and Fabris, 2015) and suggests cooling within the central west and east of the craton were not linked during the Palaeoproterozoic.

5.2. Mesoproterozoic cooling

The dominant period of cooling recorded by apatite U–Pb analysis is interpreted to be cooling following the ~1590–1580 Ma Hiltaba Event. This period of cooling is preserved in samples from the Mt. Woods Inlier, Christie Domain, Fowler Domain, and Wilgena Domain, in addition to data from the Olympic Domain. Data from Fraser et al. (2012) also preserve post-Hiltaba ages in $^{39}\text{Ar}/^{40}\text{Ar}$

samples from the central Nawa Domain. Samples from the Mt. Woods Inlier (1039419 at 1540 ± 26 Ma, 1039420 at 1404 ± 38 Ma, and 1039423 at 1472 ± 27 Ma), Christie Domain (2016111 at 1592 ± 65 Ma), and Wilgena Domain (TAR at 1539 ± 14 Ma) are from Hiltaba Granites (Daly et al., 1998; Reddy et al., 2015; Boone et al., 2016). Therefore, their apatite U–Pb ages (Table 2) are interpreted to be post-magmatic cooling following the Hiltaba Event. Samples from the Christie (0501 and 0307) and Fowler Domains (1472763 and 2017972), which formed over 100 Ma prior to the Hiltaba Event (Howard et al., 2011a; Dawson, 2016) record Hiltaba apatite U–Pb ages, indicating these samples were reheated to over ~550–350 °C during this event.

Most samples in the Nawa Domain, to the north of the Karari Shear Zone, and all samples north of the poorly known Box Hole Creek Fault (Fig. 3), preserve U–Pb ages that considerably post-date the ~1590–1560 Ma Kararan Orogeny. These U–Pb ages are consistently around ~1400–1300 Ma, and are therefore considered to have shared a similar cooling history, following their deposition and subsequent metamorphism during the Kimban

Orogeny (Payne et al., 2006; Howard et al., 2011b). In the central Nawa Domain, to the south of the Box Hole Creek Fault, Fraser et al. (2012) obtained U–Pb monazite secondary ion mass-spectrometry (SIMS) ages of 1575 ± 5 Ma. Biotite $^{40}\text{Ar}/^{39}\text{Ar}$ data from the same area yielded ages between ~ 1465 Ma and 1500 Ma (Fraser et al., 2012) and both biotite and muscovite $^{40}\text{Ar}/^{39}\text{Ar}$ data from within the Karari Shear Zone preserved ages of ~ 1440 – 1430 Ma (Fraser and Lyons, 2006; Fraser et al., 2012). These data suggest that the Nawa Domain experienced temperatures of over 550 – 350 °C until ~ 1400 – 1300 Ma, over 150 Ma after the Kararan orogeny. The samples within the central Nawa Domain, north of the Box Hill Creek Fault, preserve U–Pb ages of ~ 1400 – 1300 Ma, whereas the rocks between the Box Hill Creek Fault and the Karari Shear Zone preserve biotite $^{40}\text{Ar}/^{39}\text{Ar}$ ages of ~ 1440 – 1430 Ma. Due to the lack of apatite U–Pb data between the Box Hill Creek Fault and the Karari Shear Zone it is difficult to conclude if there is any differential cooling across the Box Hill Creek Fault. However, a potential hypothesis on the ~ 100 Ma difference in ages is that, either the north and western Nawa domain underwent greater exhumation and cooling over an extremely protracted time period after the Kararan Orogeny, or the region north of the Box Hill Creek Fault was reheated after the Kararan orogeny, possibly at ~ 1440 – 1430 Ma as strike-slip shear zone reactivation was proposed on the Karari Shear Zone by Fraser et al. (2012).

Recently, considerable middle Mesoproterozoic magmatism has been recorded in the covered basement of the far west of Gawler craton. The ~ 1490 Ma Undawidgi Supersuite in the Coompana Block (Kirkland et al., 2017) and the ~ 1415 – 1389 Ma Haig Cave Supersuite of the Madura Province, in Western Australia, record juvenile magmatism, which is thought to be a destructive plate margin on the edge of the South Australian Craton during the middle Mesoproterozoic. Similar-aged arc-magmatism and broadly coeval orogenesis also occur in the ~ 1345 – 1295 Ma Mount West Orogeny of the western Musgravites (Howard et al., 2015). This orogeny is thought to reflect the amalgamation of the previously combined South Australian and North Australian Cratons with the Western Australian Craton (Howard et al., 2015). An interpretation supported by new ages for the peak Yapunku metamorphism in the Rudall province of the far eastern Pilbara (Anderson et al., 2016) and changing provenance in the northern Australian basins at this time (Cox et al., 2016; Yang et al., submitted). We suggest that ~ 1440 – 1430 Ma reactivation of the Karari Shear Zone (Fraser et al., 2012) along with the significant heating recorded by apatite U–Pb data between this time and ~ 1300 Ma in the northern Nawa Domain reflect the foreland effects of arc-formation on the western margin of the Gawler Craton, and the subsequent collision with the Western Australian Craton.

Samples in the west of the craton, within the Fowler Domain, preserve Kararan Orogeny (~ 1530 Ma) and post-Kararan Orogeny (~ 1440 Ma) cooling. These U–Pb ages correlate well with $^{40}\text{Ar}/^{39}\text{Ar}$ from the Fowler Domain (Fraser and Lyons, 2006; Fraser et al., 2012) which are interpreted to be cooling related to movement along the Karari Shear Zone. Furthermore, Fraser et al. (2012) suggested this movement resulted in up to 10 km of exhumation in the region from the Kararan Orogeny ages. In comparison, samples along strike of the shear zones in the north-eastern Fowler Domain and Christie Domain record cooling following the Hiltaba Event. Therefore, the western Fowler Domain underwent greater exhumation from higher temperatures during the Kararan Orogeny than the centre of the craton. The younger ~ 1450 Ma ages are restricted to the Karari and Tallacootra shear zones and are interpreted to be a phase of strike-slip movement along these shear zones (Fraser and Lyons, 2006; Fraser et al., 2012). As previously suggested, the cause of

this shear zone movement is interpreted to be foreland effect of arc-formation within the far western Gawler Craton and the ensuing collision of the Western Australian Craton with the South and North Australian Cratons.

5.3. Comparisons to pre-existing $^{40}\text{Ar}/^{39}\text{Ar}$ datasets and interpolation maps

When compared to sixty $^{40}\text{Ar}/^{39}\text{Ar}$ ages from muscovite, biotite, and hornblende (~ 350 – 550 °C; McDougall and Harrison, 1999; Harrison et al., 2009) data from the northern Gawler, apatite U–Pb data preserve similar ages overall. In order to visually represent the similarities and differences in these ages and to reveal the timing and extent of tectonic events, Inverse Distance Weighted (IDW; Bartier and Keller, 1996) interpolated maps were created (Fig. 6A and B). In regions with higher data density, such as the Mt. Woods Inlier, and south-western Fowler Domain, the apatite U–Pb IDW map and $^{40}\text{Ar}/^{39}\text{Ar}$ IDW map preserve very similar ages. The two maps differ more extensively in regions where data are lacking, such as in the Nawa Domain which, due to the lack of $^{40}\text{Ar}/^{39}\text{Ar}$ data, results in a large discrepancy between the two maps. The Christie and Wilgena domains display some similarities. However, the contrasting ages of the older Mulgathong Complex and younger Hiltaba Suite coupled with the differing sampled locations between the thermochronometers ($^{40}\text{Ar}/^{39}\text{Ar}$ data and apatite U–Pb) result in the disparity between the two maps. Fig. 6B represents a more accurate temperature contour for the gap in data between the samples of the Wilgena Domain and the samples of the Olympic Domain, as this region is covered by the ~ 1590 Ma Gawler Range Volcanics (Giles, 1988; Creaser and White, 1991; Hand et al., 2007).

Overall, the $^{40}\text{Ar}/^{39}\text{Ar}$ and apatite U–Pb data correlate well, therefore, both datasets were combined into an IDW interpolated map (Fig. 7). This map identifies the rough location of major structures which played a role in the preservation of the $^{40}\text{Ar}/^{39}\text{Ar}$ and apatite U–Pb ages. For example, the rough location of the Karari Shear Zone is highlighted by younger ages (orange–red colours) curving around the north and west of the map, which is in stark contrast to the older ages (green–blue colours) within the Christie Domain, to the south. The younger fault movement within the Fowler Domain is also highlighted. To the east, the Olympic Domain is separated into cooling at ~ 1.6 Ga (green–yellow colours) and 1.7 – 1.8 Ga (blue–dark blue colours) which correlates to the locations of the ~ 1.6 Ga Hiltaba Suite and GRV to the north, and the ~ 1.8 Ga Donington Suite to the south (Fig. 1). It is important to note that in regions where the data is lacking, the IDW assumes the data is homogenous. As a result, the interpolation in these regions contain large uncertainties. More data is needed to better constrain these regions.

6. Conclusions

Apatite U–Pb data from the northern Gawler Craton preserve cooling following multiple Palaeo-Mesoproterozoic tectonic and igneous events:

- (1) Ages older than 2000 Ma record cooling of Mulgathong complex following the Sleaford Orogeny.
- (2) Central Gawler cooling is dominated by post-Kimban cooling ages of 1620 – 1670 Ma and post-Hiltaba Event cooling ages of 1600 – 1530 Ma.
- (3) Ages in the Mt. Woods Inlier are the result of post-peak metamorphism cooling and thrusting along the Southern Overthrust at around 1590 Ma during the Kararan Orogeny.

- (4) Ages within the Nawa Domain are interpreted to reflect cooling following poorly documented heating that is thought to result from the forelandward effects of arc formation on the margin of the Gawler Craton and the subsequent collision between the combined South and North Australian cratons and the Western Australia Craton at ~1450–1300 Ma.
- (5) Data from the southwestern Fowler Domain record shear zone movement at around 1440 Ma, which indicates that this region underwent greater amount of cooling and exhumation than samples along strike of the shear zones in the centre of the Gawler Craton.

Acknowledgements

This study is funded by the Geological Survey of South Australia and was made possible through an Australian Research Council grant (ARC LE150100145). Ben Wade (Adelaide Microscopy) is thanked for his assistance with the use of the LA-ICP-MS. AR publishes with permission of the director of the Geological Survey of South Australia. This paper forms TRAx#395 and is a contribution to IGCP projects 628 (Gondwana Map) and 648 (Supercontinents).

Appendix A. Supplementary data

Supplementary data related to this article can be found at <https://doi.org/10.1016/j.gsf.2017.12.010>.

References

- Allen, S.R., McPhie, J., Ferris, G., Simpson, C., 2008. Evolution and architecture of a large felsic igneous province in western Laurentia: the 1.6 Ga Gawler range volcanics, South Australia. *Journal of Volcanology and Geothermal Research* 172, 132–147.
- Anderson, J.R., Kelsey, D.E., Hand, M., Collins, W.J., 2016. Mesoproterozoic Metamorphism in the Rudall Province: Revising the Timeline of the Yapungku Orogeny and Implications for Cratonic Australia Assembly. *Australian Earth Sciences Convention*. Geological Society of Australia, Adelaide, p. 227.
- Bartier, P.M., Keller, C.P., 1996. Multivariate interpolation to incorporate thematic surface data using inverse distance weighting (IDW). *Computers & Geosciences* 22, 795–799.
- Betts, P.G., Giles, D., 2006. The 1800–1100 Ma tectonic evolution of Australia. *Precambrian Research* 144, 92–125.
- Betts, P.G., Giles, D., Foden, J., Schaefer, B.F., Mark, G., Pankhurst, M.J., Forbes, C.J., Williams, H.A., Chalmers, N.C., Hills, Q., 2009. Mesoproterozoic plume-modified orogenesis in eastern Precambrian Australia. *Tectonics* 28 n/a-n/a.
- Boone, S.C., Seiler, C., Reid, A.J., Kohn, B., Gleadow, A., 2016. An Upper Cretaceous paleo-aquifer system in the Eromanga Basin of the central Gawler Craton, South Australia: evidence from apatite fission track thermochronology. *Australian Journal of Earth Sciences* 63, 315–331.
- Budd, A.R., Fraser, G.L., 2004. Geological relationships and 40Ar/39Ar age constraints on gold mineralisation at Tarcoola, central Gawler gold province, South Australia. *Australian Journal of Earth Sciences* 51, 685–699.
- Budd, A.R., Wyborn, L.A., Bastrakova, I.V., 2001. The Metallogenic Potential of Australian Proterozoic Granites. *Geoscience Australia. Record 2001/12*.
- Butler, R.W.H., Holdsworth, R.E., Lloyd, G.E., 1997. The role of basement reactivation in continental deformation. *Journal of the Geological Society* 154, 69–71.
- Chew, D.M., Petrus, J.A., Kamber, B.S., 2014. U–Pb LA–ICPMS dating using accessory mineral standards with variable common Pb. *Chemical Geology* 363, 185–199.
- Chew, D.M., Spikings, R.A., 2015. Geochronology and thermochronology using apatite: time and temperature, lower crust to surface. *Elements* 11, 189–194.
- Chew, D.M., Sylvester, P.J., Tubrett, M.N., 2011. U–Pb and Th–Pb dating of apatite by LA–ICPMS. *Chemical Geology* 280, 200–216.
- Cowley, W.M., 2005. Solid Geology South Australia 1:2 000 000, South Australia p. map produced for St Barbara's Day Explorers Conference Primary Industries and Resources.
- Cowley, W.M., Conor, C.H.H., Zang, W., 2003. New and revised Proterozoic stratigraphic units on northern Yorke Peninsula. *Minerals and Energy South Australia Journal* 29, 46–58.
- Cowley, W.M., Fanning, C.M., 1991. Low-grade Archaean metavolcanics in the northern Gawler Craton. *Geological Survey of South Australia, Quarterly Geological Notes* 119, 2–17.
- Cox, G.M., Jarrett, A., Edwards, D., Crockford, P.W., Halverson, G.P., Collins, A.S., Poirier, A., Li, Z.-X., 2016. Basin redox and primary productivity within the Mesoproterozoic Roper Seaway. *Chemical Geology* 440, 101–114.
- Creaser, R.A., 1996. Petrogenesis of a Mesoproterozoic quartz latite-granitoid suite from the Roxby downs area, South Australia. *Precambrian Research* 79, 371–394.
- Creaser, R.A., White, A.J.R., 1991. Yardea Dacite; large-volume, high temperature felsic volcanism from the middle proterozoic of South Australia. *Geology* 19, 48–51.
- Daly, S.J., Fanning, C.M., Fairclough, M.C., 1998. Tectonic evolution and exploration potential for the Gawler Craton, South Australia. *AGSO Journal of Australian Geology and Geophysics* 17, 145–168.
- Dawson, J., 2016. Characterising Magmatic Suites in the Western Gawler Craton: Geochemical and Geochronological Constraints, *Earth Sciences*. University of Adelaide, p. 45. Unpublished.
- Direen, N.G., Cadd, A.G., Lyons, P., Teasdale, J.P., 2005. Architecture of Proterozoic shear zones in the Christie Domain, western Gawler Craton, Australia: geophysical appraisal of a poorly exposed orogenic terrane. *Precambrian Research* 142, 28–44.
- Dutch, R., Hand, M., Kinny, P.D., 2008. High-grade paleoproterozoic reworking in the southeastern Gawler Craton, South Australia. *Australian Journal of Earth Sciences* 55, 1063–1081.
- Dutch, R.A., Hand, M., Kelsey, D.E., 2010. Unravelling the tectonothermal evolution of reworked Archean granulite facies metapelites using in situ geochronology: an example from the Gawler Craton, Australia. *Journal of Metamorphic Geology* 28, 293–316.
- Ehrig, K., McPhie, J., Kamenetsky, V.S., 2012. Geology and Mineralogical Zonation of the Olympic Dam Iron Oxide Cu-U-Au-Ag Deposit, South Australia. *Society of Economic Geologists Special Publication*.
- Fairclough, M.C., Schwarz, M.P., Ferris, G.M., 2003. Interpreted Crystalline Basement Geology of the Gawler Craton. *South Australia Geological Survey, Special Map, 1:1,000,000*.
- Fanning, C.M., Flint, R.B., Parker, A.J., Ludwig, K.R., Blissett, A.H., 1988. Refined proterozoic evolution of the Gawler Craton, South Australia, through U-Pb zircon geochronology. *Precambrian Research* 40–41, 363–386.
- Fanning, C.M., Reid, A.J., Teale, G., 2007. A geochronological framework for the Gawler Craton, South Australia. *South Australia Geological Survey Bulletin* 55.
- Ferris, G., Schwarz, M., 2004. Definition of the Tunkillia suite, western Gawler craton. *Minerals and Energy South Australia Journal* 34, 32–41.
- Finlay, J., 1993. Structural Interpretation of the Mount Woods Inlier. *Monash University Melbourne, Australia (unpub)*.
- Flint, R.B., Rankin, L.R., Fanning, C.M., 1990. Definition; the palaeoproterozoic St Peter suite of the western Gawler craton. *Geological Survey of South Australia, Quarterly Geological Notes* 114, 2–8.
- Forbes, C.J., Giles, D., Hand, M., Betts, P.G., Suzuki, K., Chalmers, N., Dutch, R., 2011. Using P-T paths to interpret the tectonothermal setting of prograde metamorphism: an example from the northeastern Gawler Craton, South Australia. *Precambrian Research* 185, 65–85.
- Forbes, C.J., Giles, D., Jourdan, F., Sato, K., Omori, S., Bunch, M., 2012. Cooling and exhumation history of the northeastern Gawler Craton, South Australia. *Precambrian Research* 200–203, 209–238.
- Foster, D.A., Ehlers, K., 1998. 40Ar-39Ar thermochronology of the southern Gawler Craton, Australia: implications for Mesoproterozoic and neoproterozoic tectonics of East Gondwana and Rodinia. *Journal of Geophysical Research* 103, 10,177–110,193.
- Fraser, G., Reid, A., Stern, R., 2012. Timing of deformation and exhumation across the Karari shear zone, north-western Gawler Craton, South Australia. *Australian Journal of Earth Sciences* 59, 547–570.
- Fraser, G.L., Lyons, P., 2006. Timing of Mesoproterozoic tectonic activity in the northwestern Gawler Craton constrained by 40Ar/39Ar geochronology. *Precambrian Research* 151, 160–184.
- Fraser, G.L., Skirrow, R.G., Schmidt-Mumm, A., Holm, O., 2007. Mesoproterozoic gold in the central Gawler Craton, South Australia: geology, alteration, fluids, and timing. *Economic Geology* 102, 1511–1539.
- Giles, C.W., 1988. Petrogenesis of the proterozoic Gawler range volcanics, South Australia. *Precambrian Research* 40–41, 407–427.
- Gleadow, A.J.W., Kohn, B.P., Brown, R.W., O'Sullivan, P.B., Raza, A., 2002. Fission track thermotectonic imaging of the Australian continent. *Tectonophysics* 349, 5–21.
- Glorie, S., Agostino, K., Dutch, R., Pawley, M., Hall, J., Daníšek, M., Evans, N.J., Collins, A.S., 2017. Thermal history and differential exhumation across the Eastern Musgrave Province, South Australia: insights from low-temperature thermochronology. *Tectonophysics* 703–704, 23–41.
- Hall, J.W., Glorie, S., Collins, A.S., Reid, A., Evans, N., McInnes, B., Foden, J., 2016. Exhumation history of the Peake and Denison Inliers: insights from low-temperature thermochronology. *Australian Journal of Earth Sciences* 63, 805–820.
- Hall, J.W., Glorie, S., Reid, A.J., Collins, A.S., Jourdan, F., Evans, N., submitted. Regional thermal history of the northern Olympic Domain, Gawler Craton. *Gondwana Research*.
- Halpin, J.A., Reid, A.J., 2016. Earliest Paleoproterozoic high-grade metamorphism and orogenesis in the Gawler Craton, South Australia: the southern cousin in the Rae family? *Precambrian Research* 276, 123–144.
- Hand, M., Reid, A., Jagodzinski, L., 2007. Tectonic framework and evolution of the Gawler Craton, Southern Australia. *Economic Geology* 102, 1377–1395.
- Harrison, T.M., Célérrier, J., Aikman, A.B., Hermann, J., Heizler, M.T., 2009. Diffusion of 40Ar in muscovite. *Geochimica et Cosmochimica Acta* 73, 1039–1051.
- Howard, H.M., Smithies, R.H., Kirkland, C.L., Kelsey, D.E., Aitken, A., Wingate, M.T.D., Quentin de Gromard, R., Spaggiari, C.V., Maier, W.D., 2015. The burning heart –

- the Proterozoic geology and geological evolution of the west Musgrave Region, central Australia. *Gondwana Research* 27, 64–94.
- Howard, K.E., Hand, M., Barovich, K.M., Payne, J.L., Belousova, E.A., 2011a. U–Pb, Lu–Hf and Sm–Nd isotopic constraints on provenance and depositional timing of metasedimentary rocks in the western Gawler Craton: implications for Proterozoic reconstruction models. *Precambrian Research* 184, 43–62.
- Howard, K.E., Hand, M., Barovich, K.M., Payne, J.L., Cutts, K.A., Belousova, E.A., 2011b. U–Pb zircon, zircon Hf and whole-rock Sm–Nd isotopic constraints on the evolution of Paleoproterozoic rocks in the northern Gawler Craton. *Australian Journal of Earth Sciences* 58, 615–638.
- Jagodzinski, E., 2005. Compilation of SHRIMP U–Pb geochronological data, olympic domain, Gawler Craton, South Australia, 2001–2003. *Geoscience Australia Record* 20, 197.
- Jagodzinski, E., Reid, A.J., 2010. New zircon and monazite geochronology using SHRIMP and LA-ICPMS, from recent GOMA drilling, on samples from the northern Gawler Craton. In: Korsch, R.J., Kositcin, N. (Eds.), GOMA (Gawler Craton–Officer Basin–Musgrave Province–Amadeus Basin) Seismic and MT Workshop 2010. Geoscience Australia, pp. 108–117.
- Jagodzinski, E.A., Reid, A.J., Fraser, G., 2009. Compilation of SHRIMP U–Pb Geochronological Data for the Mulgathing Complex, Gawler Craton, South Australia, 2007–09. Department of Primary Industries and Resources, South Australia. Report Book 2009/00016.
- Kirkland, C.L., Smithies, R.H., Spaggiari, C.V., Wingate, M.T.D., Quentin de Gromard, R., Clark, C., Gardiner, N.J., Belousova, E.A., 2017. Proterozoic crustal evolution of the Eucla basement, Australia: implications for destruction of oceanic crust during emergence of Nuna. *Lithos* 278–281, 427–444.
- Korsch, R.J., Blewett, R.S., Giles, D., Reid, A.J., Neumann, N.L., Fraser, G.L., Holzschuh, J., Costelloe, R.D., Roy, I.G., Kennett, B.L.N., Cowley, W.M., Baines, G., Carr, L.K., Duan, J., Milligan, P.R., Armit, R.J., Betts, P.G., Preiss, W.V., Bendall, B.R., 2010. Geological interpretation of the deep seismic reflection and magnetotelluric line 08GA-OM1: Gawler Craton–officer basin–Musgrave Province–Amadeus Basin (GOMA), South Australia and Northern Territory. In: Korsch, R.J., Kositcin, N. (Eds.), GOMA (Gawler Craton–Officer Basin–Musgrave Province–Amadeus Basin) Seismic and MT Workshop 2010. Geoscience Australia, pp. 63–86.
- Liu, W., Zhang, J., Sun, T., Wang, J., 2014. Application of apatite U–Pb and fission-track double dating to determine the preservation potential of magnetite–apatite deposits in the Luzong and Ningwu volcanic basins, eastern China. *Journal of Geochemical Exploration* 138, 22–32.
- Ludwig, K.R., 1999. Using Isoplot/Ex, Version 2.01: a Geochronological Toolkit for Microsoft Excel. Berkeley Geochronology Center Special Publication. No. 1a: 47.
- Ludwig, K.R., 2012. User's Manual for Isoplot 3.75, A Geochronological Toolkit for Microsoft Excel. Berkeley Geochronology Center Special Publication. No. 5.
- Mark, C., Cogné, N., Chew, D., 2016. Tracking exhumation and drainage divide migration of the Western Alps: a test of the apatite U–Pb thermochronometer as a detrital provenance tool. *Geological Society of America Bulletin* 128, 1439–1460.
- McDougall, I., Harrison, M., 1999. *Geochronology and Thermochronology by the 40Ar/39Ar Method*. Oxford University Press, New York.
- McDowell, F.W., McIntosh, W.C., Farley, K.A., 2005. A precise 40Ar–39Ar reference age for the Durango apatite (U–Th)/He and fission-track dating standard. *Chemical Geology* 214, 249–263.
- McLean, M.A., Betts, P.G., 2003. Geophysical constraints of shear zones and geometry of the Hiltaba Suite granites in the western Gawler Craton, Australia. *Australian Journal of Earth Sciences* 50, 525–541.
- McPhie, J., Kamenetsky, V.S., Chambeffort, I., Ehrig, K., Green, N., 2011. Origin of the supergiant Olympic Dam Cu–U–Au–Ag deposit, South Australia: was a sedimentary basin involved? *Geology* 39, 795–798.
- Müller, W., 2003. Strengthening the link between geochronology, textures and petrology. *Earth and Planetary Science Letters* 206, 237–251.
- Oliver, R.L., Fanning, C.M., 1997. Australia and Antarctica; precise correlation of Palaeoproterozoic terrains. In: Ricci Carlo, A. (Ed.), *The Antarctic Region; Geological Evolution and Processes: Proceedings of the VII International Symposium on Antarctic Earth Sciences*. Terra Antarctica Publication, Siena, Italy, pp. 163–172.
- Parker, A.J., Daly, S.J., Flint, D.J., Flint, R.B., Preiss, W.V., Teale, G., 1993. Palaeoproterozoic. In: Drexel, J.F., Preiss, W.V., Parker, A.J. (Eds.), *The Geology of South Australia; Volume 1, the Precambrian*. South Australia Geological Survey, Bulletin 54.
- Parker, A.J., Lemon, N.M., 1982. Reconstruction of the early proterozoic stratigraphy of the Gawler craton, South Australia. *Journal of the Geological Society of Australia* 29, 221–238.
- Paton, C., Hellstrom, J., Paul, B., Woodhead, J., Hergt, J., 2011. Iolite: freeware for the visualisation and processing of mass spectrometric data. *Journal of Analytical Atomic Spectrometry* 26, 2508–2518.
- Payne, J.L., Barovich, K.M., Hand, M., 2006. Provenance of metasedimentary rocks in the northern Gawler Craton, Australia: implications for palaeoproterozoic reconstructions. *Precambrian Research* 148, 275–291.
- Payne, J.L., Hand, M., Barovich, K.M., Wade, B.P., 2008. Temporal constraints on the timing of high-grade metamorphism in the northern Gawler Craton: implications for assembly of the Australian Proterozoic. *Australian Journal of Earth Sciences* 55, 623–640.
- Pochon, A., Poujol, M., Gloaguen, E., Branquet, Y., Cagnard, F., Gumiaux, C., Gapais, D., 2016. U–Pb LA-ICP-MS Dating of Apatite in Mafic Rocks: Evidence for a Major Magmatic Event at the Devonian-Carboniferous Boundary in the Armorican Massif (France). *American Mineralogist*, p. 2430.
- Rankin, L.R., Flint, R.B., Fanning, C.M., 1990. Palaeoproterozoic Nuyts Volcanics of the Western Gawler Craton, South Australia. Department of Primary Industries and Resources, p. 17. Report Book 90/60.
- Rankin, L.R., Martin, A.R., Parker, A.J., 1989. Early proterozoic history of the Karari fault zone, northwest Gawler Craton, South Australia. *Australian Journal of Earth Sciences* 36, 123–133.
- Reddy, M., Glorie, S., Reid, A.J., Collins, A.S., 2015. Phanerozoic cooling history of the central Gawler Craton: implications of new low-temperature thermochronological data. *MESA Journal* 75, 56–60.
- Reddy, S.M., Potts, G.J., 1999. Constraining absolute deformation ages: the relationship between deformation mechanisms and isotope systematics. *Journal of Structural Geology* 21, 1255–1265.
- Reid, A., Hand, M., Jagodzinski, E., Kelsey, D., Pearson, N., 2008. Paleoproterozoic orogenesis in the southeastern Gawler Craton, South Australia. *Australian Journal of Earth Sciences* 55, 449–471.
- Reid, A.J., Fabris, A., 2015. Influence of preexisting low metamorphic grade sedimentary successions on the distribution of iron oxide copper-gold mineralization in the olympic Cu-Au Province, Gawler Craton. *Economic Geology* 110, 2147–2157.
- Reid, A.J., Fricke, C.E., Cowley, W.M., 2009. Extent of low-grade Archaean metavolcanics in the northeastern Gawler Craton: new evidence and definition of the devils playground volcanics. *MESA Journal* 054, 009–019.
- Reid, A.J., Jagodzinski, E.A., Fraser, G.L., 2010. New constraints on the tectonics of the Archaean–palaeoproterozoic transition from the Gawler Craton, South Australia. In: M., T.I., M., K.-R.C. (Eds.), *Fifth International Archean Symposium Abstracts*. Geological Survey of Western Australia, p. 203. Record 2010/18.
- Reid, A.J., Jagodzinski, E.A., Fraser, G.L., Pawley, M.J., 2014. SHRIMP U–Pb zircon age constraints on the tectonics of the neorarchean to early paleoproterozoic transition within the Mulgathing complex, Gawler Craton, South Australia. *Precambrian Research* 250, 27–49.
- Reid, A.J., Jourdan, F., Jagodzinski, E.A., 2017. Mesoproterozoic fluid events affecting Archean crust in the northern Olympic Cu–Au Province, Gawler Craton: insights from 40Ar/39Ar thermochronology. *Australian Journal of Earth Sciences* 64, 103–119.
- Shaw, C.A., Karlstrom, K.E., Williams, M.L., Jercinovic, M.J., McCoy, A.M., 2001. Electron-microprobe monazite dating of ca. 1.71–1.63 Ga and ca. 1.45–1.38 Ga deformation in the Homestake shear zone, Colorado: origin and early evolution of a persistent intracontinental tectonic zone. *Geology* 29, 739–742.
- Skirrow, R.G., Bastrakov, E.N., Davidson, G.J., Raymond, O.L., Heathersay, P., 2002. The geological framework, distribution and controls of Fe-oxide and related alteration, and Cu–Au mineralisation in the Gawler craton, South Australia. Part II: alteration and mineralisation. In: Porter, T.M. (Ed.), *Hydrothermal Iron Oxide Copper-gold and Related Deposits: A Global Perspective*, 2. Porter Ge-Consultancy Publishing, Adelaide, pp. 33–47.
- Stewart, A.J., Betts, P.G., Collins, A.S., Schaefer, B.F., 2009. Multi-scale analysis of Proterozoic shear zones: an integrated structural and geophysical study. *Journal of Structural Geology* 31, 1238–1254.
- Stewart, J.R., Betts, P.G., 2010. Implications for Proterozoic plate margin evolution from geophysical analysis and crustal-scale modeling within the western Gawler Craton, Australia. *Tectonophysics* 483, 151–177.
- Swain, G.M., Hand, M., Teasdale, J., Rutherford, L., Clark, C., 2005. Age constraints on terrane-scale shear zones in the Gawler Craton, southern Australia. *Precambrian Research* 139, 164–180.
- Szpunar, M., Hand, M., Barovich, K., Jagodzinski, E., Belousova, E., 2011. Isotopic and geochemical constraints on the paleoproterozoic Hutchison Group, southern Australia: implications for paleoproterozoic continental reconstructions. *Precambrian Research* 187, 99–126.
- Teasdale, J., 1997. The Interpretive Geology and Tectonothermal Evolution of the Western Gawler Craton. Ph.D. thesis. University of Adelaide, pp. 1–142. Unpublished.
- Thomson, S.N., Gehrels, G.E., Ruiz, J., Buchwaldt, R., 2012. Routine low-damage apatite U–Pb dating using laser ablation–multicollector–ICPMS. *Geochemistry, Geophysics, Geosystems* 13.
- Tomkins, A.G., Dunlap, W.J., Mavrogenes, J.A., 2004. Geochronological constraints on the polymetamorphic evolution of the granulite-hosted Challenger gold deposit: implications for assembly of the northwest Gawler Craton*. *Australian Journal of Earth Sciences* 51, 1–14.
- Tomkins, A.G., Mavrogenes, J.A., 2002. Mobilization of gold as a polymetallic Melt during pelite Anatexis at the challenger deposit, South Australia: a meta-morphosed Archean gold deposit. *Economic Geology* 97, 1249–1271.
- Williams, H.A., Betts, P.G., 2009. The Benareger Shear Zone: 1100 Myr of reactivation history and control over continental lithospheric deformation. *Gondwana Research* 15, 1–13.
- Yang, B., Smith, T., Collins, A.S., Munson, T.J., Schoemaker, B., Nicholls, D., Cox, G., Farkas, J., Glorie, S., submitted. Spatial and temporal detrital zircon U–Pb provenance of the hydrocarbon-bearing upper Roper Group, Beetaloo Sub-basin, Northern Territory, Australia. *Precambrian Research*.
- Zattin, M., Andreucci, B., Thomson, S.N., Reiners, P.W., Talarico, F.M., 2012. New constraints on the provenance of the ANDRILL AND-2A succession (western Ross Sea, Antarctica) from apatite triple dating. *Geochemistry, Geophysics, Geosystems* 13 n/a-n/a.
- Zhang, F., Wang, X., Sun, Z., Chen, X., Zhou, X., Yang, T., 2017. Geochemistry and zircon–apatite U–Pb geochronology of mafic dykes in the Shuangxiu area: constraints on the initiation of Neoproterozoic rifting in South China. *Precambrian Research* [in press].